A single-loop time-variant reliability evaluation via a decoupling strategy and probability distribution reconstruction

Yang Zhang[a], Jun Xu[a,b,*], Michael Beer[c,d,e]

[a] *College of Civil Engineering, Hunan University, Changsha, 410082, P.R.China.*
[b] *Key Lab on Damage Diagnosis for Engineering Structures of Hunan Province, Hunan University, 410082, P.R.China*
[c] *Institute for Risk and Reliability, Faculty of Civil Engineering and Geodetic Science, Leibniz University Hannover, Callinstr. 34, 30167 6 Hannover, Germany*
[d] *Institute for Risk and Uncertainty and School of Engineering, University of Liverpool, Peach Street, Liverpool L69 7ZF, United Kingdom*
[e] *International Joint Research Center for Engineering Reliability and Stochastic Mechanics, Tongji University, No. 1239, Si Ping Rd. Shanghai 9 200092, PR China*

Abstract

In this paper, a single-loop approach for time-variant reliability evaluation is proposed based on a decoupling strategy and probability distribution reconstruction. The most attractive feature of the proposed method is that the reliability at a specified time instant can be captured by performing time-invariant reliability analysis only once. In this method, the expansion optimal linear estimation is first employed to discretize the loading stochastic process. Then, a decoupling strategy that decouples the loading stochastic process and degradation processes is developed to formulate a single-loop method for time-variant reliability analysis, where an equivalent extreme value limit state function (EEV-LSF) is obtained. To improve the accuracy and robustness, the Box-Cox transformation is applied to get a transformed EEV-LSF. The maximum entropy method with fractional exponential moments is employed to robustly derive the probability distribution of transformed EEV-LSF. Once the probability distribution is captured, the time-variant failure probability can be readily computed. To handle a large number of random variables, a weighted sampling method is applied for moment assessment to ensure an efficient solution. Numerical examples including a complex real-world case are studied to validate the proposed method, where pertinent Monte Carlo simulations and PHI2 method are conducted for comparisons.

Keywords: Time-variant reliability; Decoupling strategy; Box-Cox transformation; Fractional exponential moments; Maximum entropy method; Voronoi cells

---

1. Introduction

In engineering practices, many factors may exhibit time-variant characteristics, e.g., the structural resistance may deteriorate due to aging under the aggressive service environment [1, 2, 3], and the external loadings may also vary with time. Therefore, time-variant reliability analysis of structures is of paramount importance and gains increasing attention in the reliability community [4, 5, 6, 7, 8, 9, 10], which is generally more complicated than the time-invariant problems since the effect of time factor cannot be ignored. Usually, two possible failure modes exist for time-variant reliability analysis of structure, which are the first-passage failure and damage accumulation as in fatigue [11, 12, 13]. In this paper, only the first-passage failure mode is considered, where the methods can be categorized into two main groups: the out-crossing rate approaches and extreme value distribution (EVD)-based approaches.

For the first-passage failure, the out-crossing rate measure of stochastic process over the prescribed threshold is always of great concern [14, 15, 16]. Numerous approaches have been developed in the literature to compute the out-crossing rate using the asymptotic integration [17, 18, 19]. Rice's formula [14] could be one of the most commonly used approaches, which assumes all crossing events are independent. Then, several improvements on Rice's formula have been developed [15, 20, 21, 22, 23]. The representative contribution is the PHI2 method [15], which computes the out-crossing rate in time-variant reliability problem by using a classical time-invariant parallel system composed of a pair of limit state functions (LSFs) at successive time instants. Then, the out-crossing rate is approximated by the bivariate normal integral using the first-order reliability method (FORM) [24]. Some improved PHI2-based methods have been developed recently. For example, a moment-based PHI2 method is proposed to improve the efficiency by separating finite element analysis from the time-variant reliability analysis cycle [25]. To avoid the two-dimensional numerical integration required in PHI2 method, an explicit model of the out-crossing rate is put forward to improve the computational efficiency [26]. Although the out-crossing rate approach is quite efficient for time-variant reliability problems, some inherent deficiencies still exist, e.g., the Poisson distribution

*Corresponding author
Email addresses: zhangyang98@hnu.edu.cn (Yang Zhang), xujun86@hnu.edu.cn (Jun Xu), beer@irz.uni-hannover.de (Michael Beer)

assumption of crossing events, and the limitations of FORM, which hinder their applications to general cases.

Alternatively, the EVD-based approaches are developed to address the time-variant reliability problems, where the extreme value of a time-variant LSF is extracted as a measure to quantify the reliability. The surrogate model or probability density function (PDF) is constructed to characterize the extreme value of time-variant LSF in a specified time duration, where the time-variant problem is actually converted to be a time-invariant counterpart. Then, the existing time-invariant reliability tools can be incorporated for time-variant reliability approximation [27]. Many efforts are devoted to developing the surrogate model for the extreme value of response, e.g., the nested extreme value response method [28], mixed global optimization method with adaptive Kriging Monte Carlo simulation (MCS) [29], confidence-based adaptive extreme response surface method [30], polynomial chaos expansion with dimension reduction [31], a method combining multiple response Gaussian process and subset simulation [32], and a method combining multiple response Gaussian process and Kriging model [33], etc. However, if the LSF involves stochastic processes, the total number of input random variables increases significantly due to the discretization of stochastic processes. In that regard, a large number of computational efforts are necessary, which makes the surrogate models inefficient for time-variant reliability analysis. The computational efforts and accuracy of the surrogate model may suffer from the so-called "curse of dimensionality", as the number of variables and the nonlinearity in the problem increases [34]. The other route of the EVD-based approaches is to reconstruct the PDF of extreme value at each time instant, which can be used to straightforwardly evaluate the time-variant failure probabilities. In Ref. [35], a sampling approach and saddle point approximation are employed to obtain the EVD, where a large sample size is still required to ensure accuracy. The time-variant EVD evolution method is developed based on its first-four central moments [36], however, the accuracy may become quite poor for general cases due to the inherent univariate dimension-reduction method. Besides, it should be emphasized that the aforementioned EVD-based approaches involve double-loop computations for time-variant reliability analysis, where significant computational efforts are actually indispensable.

On the other hand, the structural performance could deteriorate as a result of the action of regular operating or environmental conditions in service, which also needs to be taken into account in time-variant reliability analysis. Structural degradation mechanisms are often divided into two categories: progressive degradation and shock degradation [37]. In the past decades, many researchers devote to modeling the structural degradation [37, 38, 39, 40, 41, 42]. In the field of time-variant reliability analysis, if repair or maintenance measures are not involved, structural degradation processes are often treated as monotonically non-increasing and are modeled as deterministic functions or stochastic functions [3, 28, 29, 43, 44]. In this paper, only the progressive degradation processes, which are modeled by the monotonically non-increasing deterministic functions are considered [3, 15, 45].

When the degradation processes and loading stochastic process are simultaneously considered, which are actually coupled, the EVD-based approaches are generally applicable for time-variant reliability analysis. However, as mentioned, a large amount of computational efforts are still required since a double-loop problem is involved. It is difficult to extract the EVD over the concerned time period in an efficient manner due to the coupling. Considering the limitations above, a single-loop method for time-variant reliability analysis will be proposed with high efficiency and accuracy in the present paper. In the proposed method, a decoupling strategy is first put forward to decouple the loading stochastic process and degradation processes. In that regard, the double-loop time-variant reliability problem can be avoided, whereby a single-loop problem is actually formulated. A transformed EEV-LSF over the concerned time period is then of great concern. The PDF of transformed EEV-LSF is recovered by using the fractional exponential moments-based maximum entropy method (FEM-MEM) with accuracy and efficiency. Finally, the time-variant failure probability can be obtained by integrating the estimated PDF over the failure domain, where a time-invariant reliability analysis procedure is implemented. It should be emphasized that the most attractive feature of the proposed method is that the time-invariant reliability analysis of structures is performed only once to obtain the failure probability over the concerned time period. In that regard, the computational time can be greatly saved compared to the double-loop approaches. It is worth pointing out that the proposed method cannot deal with time-variant reliability problems involving the stochastic degradation process. The rest of the paper is organized as follows. In **Section 2**, the problem statement of time-variant reliability analysis and the EVD-based method are briefly revisited. Then, the so-called decoupling strategy is proposed to improve the efficiency for calculating the extreme value of response for time-variant LSF in **Section 3.1**. In **Section 3.2**, the PDF derivation of a transformed EEV-LSF is presented, where the Box-Cox transformation, FEM-MEM, and a weighted sampling method are involved. In **Section 4**, three numerical examples are investigated to demonstrate the accuracy and efficiency of the proposed method. The last section contains the concluding remarks.

2. Time-variant reliability analysis

2.1. Problem formulation

Time-variant reliability of a structure refers to the probability that the structure can fulfill an intended function within a specified time period under intended conditions with consideration of the effect of time-dependent uncertainty. Let $Z(t) = G(\mathbf{X}, Y(t), t)$ denotes the time-variant limit state function (LSF), where $\mathbf{X} = [X_1, X_2, \cdots, X_d]$ represents the d time-invariant random variables related to structural properties, e.g., component size, material properties, etc., and $Y(t)$ is an input scalar stochastic process with the time t, which collects time-variant loadings. In this paper, it is assumed that the stochastic process is used to only refer to the loading process and stochastic process and random variables are all independent with each other. For a specified time period $[0, t_c]$, the structural failure occurs if the LSF is less than zero at a time instant t, $t \in [0, t_c]$. Then, the time-variant failure probability within the time interval $[0, t_c]$, denoted as $P_f(0, t_c)$, can be defined as

$$P_f(0, t_c) = \Pr\{\exists t \in [0, t_c], G(\mathbf{X}, Y(t), t) < 0\} \tag{1}$$

As a result, the time-variant reliability can be written as

$$R(0, t_c) = 1 - P_f(0, t_c) \tag{2}$$

It is technically intractable to derive a closed-form solution for evaluating the time-variant failure probability since the correlation of structure failures at different time instants could be involved [27]. For numerical solutions, the input loading stochastic process must be explicitly represented as the function of time and random variables. Various approaches have been developed to obtain the explicit representation of stochastic process such as the expansion optimal linear estimation (EOLE) [46, 47], orthogonal series expansion (OSE) [48] and Karhunen-Loeve (KL) expansion [49, 50, 51, 52], etc. In the present paper, the EOLE method is specifically adopted for simulating the loading stochastic process.

2.2. Decomposition of loading stochastic process via EOLE

Consider the Gaussian loading stochastic process, namely $Y(t)$, which can be completely characterized by its mean value $m(t)$, standard deviation $\sigma(t)$ and autocorrelation coefficient $\rho_Y(t, t_i)$. In order to discretize the process, L time instants $t_i = i\Delta t,\ \Delta t = t_c/L,\ i = 1, 2, \cdots, L$, are selected from the considered time interval $[0, t_c]$, t_c is the time duration. Then, the loading stochastic process $Y(t)$ can be approximately represented by EOLE such that [47]

$$Y(t) \approx \tilde{Y}(t) = m(t) + \sigma(t) \sum_{h=1}^{M} \frac{\Xi_h}{\sqrt{\chi_h}} \phi_h^{\mathrm{T}} C_{Y,t,t_k}(t) \tag{3}$$

where M is the truncated order of the EOLE for $Y(t)$, corresponding to the M largest eigenvalues of the correlation matrix $\mathbf{C}$, whose generic term is $C_{kp} = \{\rho_Y(t_k, t_p),\ k, p = 1, \cdots, L\}$, Ξ_h are the independent standard normal random variables, χ_h and ϕ_h are the eigenvalues and eigenvectors of $\mathbf{C}$, and $C_{Y,t,t_k}(t)$ is a time-variant vector, whose components are $C_{Y,t,t_k}(t) = \{\rho_Y(t, t_k),\ k = 1, \cdots, L\}$.

It is known that truncation error decreases monotonically as the number of terms M increases. An error estimator [15], which allows evaluating the accuracy of the discretization is given by:

$$\mathrm{err}(t) = 1 - \sum_{h=1}^{M} \frac{1}{\chi_h} \left(\phi_h^{\mathrm{T}} C_{Y,t,t_k}(t)\right)^2 \tag{4}$$

where the number of terms M can be determined by $\mathrm{err}(t) < 10^{-2}$.

Based on the procedure above, the original time-variant LSF can be expressed in terms of only random variables and time such that $G(\mathbf{X}, \boldsymbol{\Xi}, t)$, where $\boldsymbol{\Xi} = [\Xi_1, \Xi_2, \cdots, \Xi_M]$ and the total number of random variables is $D = d + M$. It is known that the truncated order of EOLE is always quite large, e.g., $M > 10$, to secure an acceptable accuracy for the simulation of a loading stochastic process. That means the total number of random variables in $G(\mathbf{X}, \boldsymbol{\Xi}, t)$ could be also very large, which results in the "curse of dimensionality" and brings a tremendous computational burden for time-variant reliability analysis.

2.3. EVD-based approach

The EVD-based approach is a popular approach for time-variant reliability analysis. In such an approach, the extreme values of response of a structure over a specified time period are extracted for time-variant reliability analysis [27]. According to the extreme value theorem in Ref. [53], the time-variant LSF at each time instant could also be regarded as a random variable. The equivalent extreme value (EEV) [53] of time-variant LSF $G(\mathbf{X}, \boldsymbol{\Xi}, t)$ over the time period $[0, t_c]$ can be expressed as

$$W_{\min}(\mathbf{X}, \boldsymbol{\Xi}, t_c) = \min_{t \in [0, t_c]} \{G(\mathbf{X}, \boldsymbol{\Xi}, t)\} \tag{5}$$

where $W_{\min}$ denotes the EEV of $G(\mathbf{X}, \boldsymbol{\Xi}, t)$. Therefore, if $W_{\min} > 0$ always holds over the time period $[0, t_c]$, the structure is in the safe domain; otherwise, the structural failure occurs.

In that regard, the PDF of the extreme value $W_{\min}$ is of great concern for time-variant reliability analysis. Once the PDF of $W_{\min}$ is available, the time-variant failure probability can be readily obtained by

$$P_f(0, t_c) = \int_{-\infty}^{0} p_{W_{\min}}(w, t_c)\, \mathrm{d}w \tag{6}$$

where $p_{W_{\min}}(w, t_c)$ denotes the EVD during the time period $[0, t_c]$.

Although the EVD-based approach is effective and has been widely applied for time-variant reliability analysis, it is generally necessary to perform the LSF evaluations at each discrete time instant to extract the EVD for time-variant reliability analysis, where a double-loop problem is actually involved. Therefore, if one concerns the failure probability at a specific time instant, the model calculations before this time instant all need to be implemented, where multiple-round reliability analyses need to be implemented and significant computational efforts could be necessary.

3. The proposed single-loop method for structural time-variant reliability analysis

To avoid the thorny double-loop problem, a single-loop time-variant reliability evaluation method based on a decoupling strategy and probability distribution reconstruction will be developed in this section. In the proposed method, a decoupling strategy of loading stochastic process and degradation processes involved in time-variant reliability analysis is first proposed to convert the double-loop problem into a single-loop problem. In that regard, only by performing a single-round time-invariant reliability analysis at the concerned time instant, the corresponding time-variant failure probability can be obtained accordingly. It should be emphasized that one does not need to perform reliability analysis at any moment before the concerned time instant during this process, indicating the computational time can be greatly saved for time-variant reliability analysis.

In the proposed method, the EOLE is applied for simulating the loading stochastic process. A weighted sampling method is then employed to generate the samples of loading stochastic process and random variables. The decoupling strategy is then implemented to decouple the samples of loading stochastic process and degradation processes, where the samples related to the extreme value of response at the concerned time instant can be obtained. Based on these samples, the FEM-MEM is employed to derive the PDF related to the extreme value of response, where the EVD-based approach can be applied to estimate the time-variant reliability. For a clear illustration, the flowchart of the proposed method for time-variant reliability analysis is illustrated in Figure 1. In addition, the detailed steps are also outlined as follows:

Step 1 : Determine the number of truncated term M in the stochastic process $Y(t)$ according to the error estimation formula (Eq. (4)), and specify the total number of variables $D = d + M$ involved in both structural properties and loadings.

Step 2 : Implement the weighted sampling strategy (Section 3.2.3) to generate the points and weights for the high-dimensional independent standard normal space, where the points and weights for the original probability space can be specified accordingly.

Step 3 : Substitute the points into Eq. (3) to discretize the loading stochastic process $Y(t)$ and obtain the corresponding samples of maximal value process (MVP), denoted as $V(t)$, and degradation processes, denoted as $\mathbf{D}(t)$.

Step 4 : Perform the decoupling strategy in Section 3.1 to decouple the MVP $V(t)$ and degradation processes $\mathbf{D}(t)$. Then, the corresponding samples of $\mathbf{X}$, MVP $V(t)$ and the new degradation processes, denoted as $\mathbf{D}(\bar{t})$, are substituted into Eq. (18) to calculate the samples of the concerned function $\eta(\mathbf{X}, \mathbf{D}(\bar{t}), V(t), t)$ at any time instant of interest, where deterministic LSF calls are performed.

Step 5 : Implement the Box-Cox transformation (Sect. 3.2.1) to transform the original EEV-LSF, denoted as $g(\mathbf{X}, \mathbf{D}(\bar{t}), V(t), t)$, into a normal or weakly non-normal distributed EEV-LSF $\tilde{g}(\mathbf{X}, \mathbf{D}(\bar{t}), V(t), t)$. Then, the samples of $\tilde{g}(\mathbf{X}, \mathbf{D}(\bar{t}), V(t), t)$ can be directly obtained.

Step 6 : Carry out the FEM-MEM in Section 3.2.2 to obtain the PDF of $\tilde{g}(\mathbf{X}, \mathbf{D}(\bar{t}), V(t), t)$, in which the FEMs are computed by the samples in Step 5.

Step 7 : Calculate the failure probability at the concerned time instant by integrating the corresponding PDF over the failure domain (Eq. (19)).

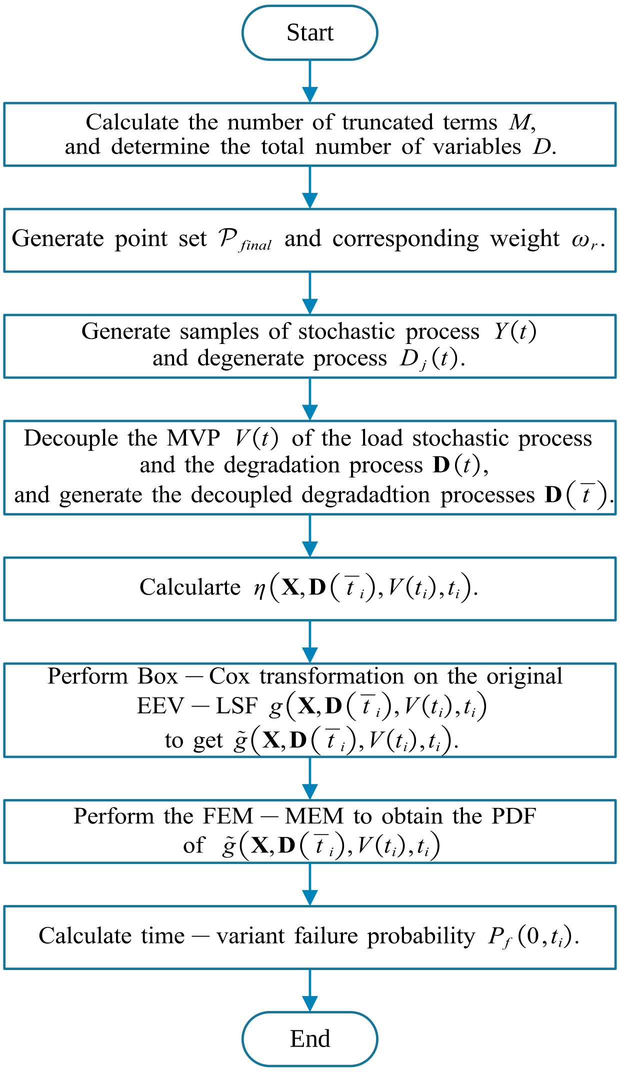

Figure 1: Flowchart of the proposed method for time-variant reliability analysis

3.1. *Decoupling strategy of loading stochastic process and degradation processes*

In engineering practice, structural degradation has effects on both the structural resistance and loading effect [39]. Without loss of generality, the time-variant LSF of structures can be also expressed as:

$$G\left(\mathbf{X}, \mathbf{D}\left(t\right), Y\left(t\right), t\right) = R\left(\mathbf{X}, \mathbf{D}\left(t\right), t\right) - S\left(\mathbf{X}, \mathbf{D}\left(t\right), Y\left(t\right), t\right) \tag{7}$$

where $R\left(\mathbf{X}, \mathbf{D}\left(t\right), t\right)$ and $S\left(\mathbf{X}, \mathbf{D}\left(t\right), Y\left(t\right), t\right)$ denote the structural resistance and loading effect, respectively; and $\mathbf{D}\left(t\right)$ represents the monotonically non-increasing degradation processes of the structure.

The degradation processes, such as the strength degradation, and loading stochastic process are actually coupled in time-variant reliability analysis. The degradation processes involved in this paper are independent and progressive and are modeled by deterministic functions. Besides, since the time-variant loads considered in the paper are long-term ones (over years) rather than short-term time-variant loads, such as earthquake and wind loads, the dynamic effects, i.e., the inertial and damping forces, are not considered in this paper, where a series of static problems at each time instant are actually involved in time-variant reliability analysis. In this regard, the first-passage of load effect over structural resistance still indicates structural failure, whereby the first-passage failure probability is concerned [15, 22]. Then, it is known that the changes in structural response are synchronized with the changes in the loading process applied to the structure when the degradation processes are not considered. In other words, the extreme value of response actually occurs along with the extreme value of time-variant loading process at the same time when the degradation processes are not involved. This feature provides us an opportunity to transform the time-variant problem into the corresponding time-invariant one, where the extreme value of response over the concerned time interval could be extracted by simply performing the LSF evaluations at the final time instant. The extreme value of loading stochastic process over the concerned time interval is first obtained, which is then applied to the structure to perform model evaluations and capture the extreme value of response during the time interval. Since extracting the extreme value of loading stochastic process does not involve deterministic model evaluations, a single-loop problem is actually performed to obtain the EVD of response during the time interval, where only a single-round reliability analysis is readily implemented.

From the relationship between the principle of first-passage failure and the extreme response, it is known that the structure fails when the extreme value of response reaches its prescribed threshold for the first time during the service life. Actually, the maximum value of response is always considered as the extreme response for structural failure identification, which is referred to as the maximum failure assumption. Therefore, one needs to calculate the maximal value process (MVP) of a loading stochastic process [54] before implementing the decoupling strategy to obtain the maximum value of response. Consider a positive loading stochastic process $Y(t)$, the corresponding MVP can be defined as

$$V(t) = \max_{0 \leq \tau \leq t} \{Y(\tau)\} \tag{8}$$

A sketch of the relation between $Y(t)$ and $V(t)$ is shown in Figure 2. Since $Y(t)$ is a stochastic process, $V(t)$ is also a stochastic process which is monotonically non-decreasing in the sample sense.

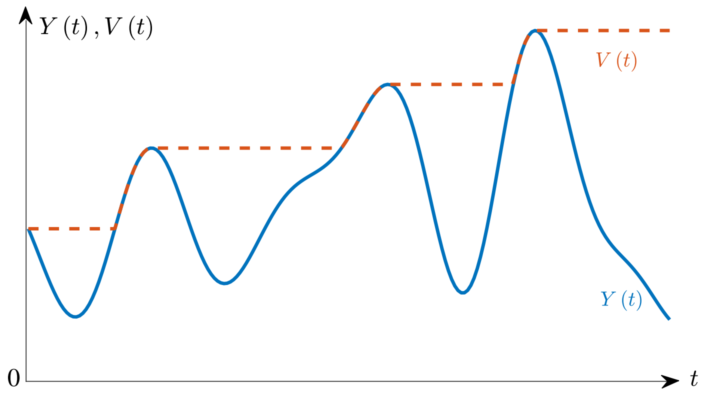

Figure 2: Sketch of the MVP $V(t)$ and the underlying loading stochastic process $Y(t)$

As mentioned above, the changes in structural response are consistent with the changes in the loading process applied to the structure without consideration of degradation processes. Therefore, after obtaining the MVP of loading stochastic process, it is directly applied to the structure to obtain the extreme value of response at any time instant, where only one-round model evaluations at that time instant is involved. Contrary to the traditional scheme of extracting the extreme value of time-variant response in EVD-based approaches, this strategy does not need the model evaluations before this time instant, which could significantly reduce the computational efforts.

However, the maximum load does not necessarily lead to the maximum response when the degradation processes are involved. Therefore, another thorny problem, how to decouple the degradation processes from the loading stochastic process, needs to be addressed. Let $\mathbf{D}(t) = [D_1(t), D_2(t), \cdots, D_m(t)]$ denote the degradation processes involved in time-variant reliability analysis. In engineering practice, it is reasonable to assume that structural resistance actually decreases slowly with time, where the slope change of a degradation process is not quite large. It could be imprudent to directly use the degradation values of structural resistance together with the extreme value of response at a specific time instant t_c to compute the time-variant failure probability. As shown in Figure 3, it is seen that the structure does not fail at the concerned time instant t_c since the structural resistance $R(\mathbf{X}, \mathbf{D}(t), t)$ is always larger than the load effect $S(\mathbf{X}, \mathbf{D}(t), Y(t), t)$ in this time interval $[0, t_c]$. However, when the extreme value of load effect $S\left(\mathbf{X}, \mathbf{D}\left(\tilde{t}\right), V\left(\tilde{t}\right), t_c\right)$ and structural resistance $R(\mathbf{X}, \mathbf{D}(t_c), t_c)$ at this time instant t_c are extracted to judge whether the structure is of failure or not, a wrong judgment could be arrived, where the structure fails at this time instant. This is because, from the time instant $\tilde{t}$, where the extreme value of load effect first occurs, the maximum load $V\left(\tilde{t}\right)$, where $V\left(\tilde{t}\right) = V(t_c)$, and degradation processes $\mathbf{D}\left(\tilde{t}\right)$ has been used to calculate the extreme value of response, but the structural resistance constantly decreases, which leads to the misjudgment of failure events. From the facts above, in order to efficiently and reasonably evaluate the time-variant reliability of a structure through a single-loop method, it is necessary to perform a decoupling strategy for the degradation processes and loading stochastic process.

Since it is impossible to correctly judge whether the structure fails at the current time instant only through the MVP of loading process and degradation values of structural resistance at that moment, the time-variant failure probability of the structure cannot be calculated correctly. Therefore, one needs to identify the degradation values $\mathbf{D}(\bar{t})$ corresponding to $V(t)$ from $\mathbf{D}(t)$, instead of directly substituting $\mathbf{D}(t)$ into the LSF for the calculation, that is, implementing the so-called decoupling strategy, where $\mathbf{D}(\bar{t}) = [D_1(\bar{t}), D_2(\bar{t}), \cdots, D_m(\bar{t})]$. The crucial issue is to identify the time instant $\bar{t}$ when $Y(t)$ equals the extreme value $V(t_c)$ for the last time, and to use the degradation values $\mathbf{D}(\bar{t})$ at the time instant $\bar{t}$ for the structural resistance and load effect as the basis corresponding to the first-passage failure. The following will

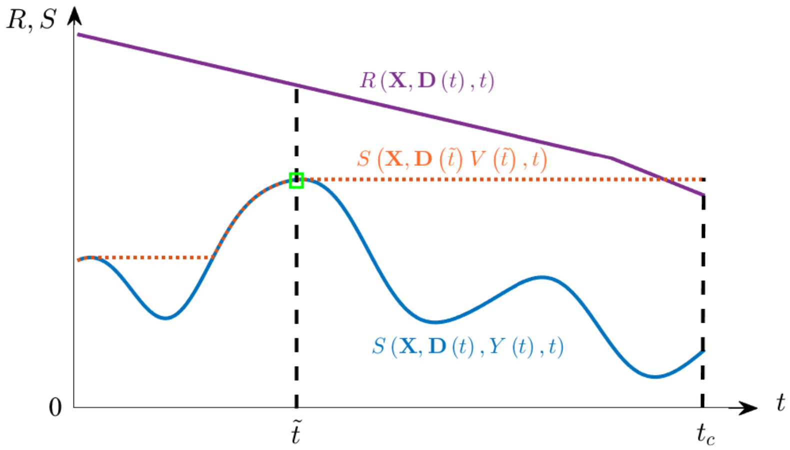

Figure 3: Schematic diagram of $R(\mathbf{X}, \mathbf{D}(t), t)$, $S\left(\mathbf{X}, \mathbf{D}\left(\tilde{t}\right), V\left(\tilde{t}\right), t\right)$ and $S(\mathbf{X}, \mathbf{D}(t), V(t), t)$

describe how to obtain $\mathbf{D}(\bar{t})$ step by step in detail from the sample perspective. For ease of understanding, the following steps take the time-variant failure probability $P_f(0, t_c)$ at the time instant t_c as an illustrative example and the time-variant failure probability at any other time instant can be similarly deduced.

Step 1 : Calculate the value $V(t_c)$ of the load MVP at the time instant t_c, which is illustrated as the process ① in Figure 4, where the coordinate of point b in Figure 4 is $(t_c, V(t_c))$.

Step 2 : Record all the discrete time instants when $Y(t)$ equal to $V(t_c)$ to form a time vector $\tilde{T}_c$, where $\tilde{T}_c = \left[\tilde{t}_{c,1}, \cdots, \tilde{t}_{c,i}, \cdots \tilde{t}_{c,l}\right]$, $1 \leq i \leq l, 1 \leq l \leq L$. Then, specify the maximum value of $\tilde{T}_c$ and record it as $\bar{t}_c$:

$$\tilde{T}_c \quad = \left[\tilde{t}_{c,1}, \cdots, \tilde{t}_{c,i}, \cdots \tilde{t}_{c,l}\right] = \underset{\tilde{t}_{c,i} \in [t_1, t_2, \cdots, t_L]}{\arg\ \min} \left(\left|Y\left(\tilde{t}_{c,i}\right) - V(t_c)\right|\right) \tag{9}$$

$$\bar{t}_c = \max\left\{\tilde{T}_c\right\} \tag{10}$$

where $V(t_c)$ refers to the realization value of $V(t)$ at the time instant t_c and $Y\left(\tilde{t}_{c,i}\right)$ is the realization sample of stochastic process $Y(t)$. It can be more intuitively understood in combination with Figure 4. This step involves the processes ② and ③ in Figure 4. In practical situations, there may be multiple discrete moments $\tilde{t}_{c,i}$ such that $Y(t)$ equals to $V(t_c)$, such as $\tilde{t}_{c,1}$ and $\tilde{t}_{c,2}$ in Figure 4. In this case, the relatively larger value of these time instants needs to be taken as $\bar{t}_c$, that is, $\bar{t}_c = \tilde{t}_{c,2}$. Actually, $\bar{t}_c$ is a random quantity in essence. Since the sample perspective is considered for the illustration, $\bar{t}_c$ is treated as an intermediate quantity to determine the sample values of $\mathbf{D}\left(\bar{t}_c\right)$.

The reason for performing this step is that the smallest structural resistance corresponding to its loading MVP needs to be correctly identified at the time instant $\bar{t}_c$. When the structure is still of safety at $\bar{t}_c$, it can be deduced that the structure does not experience failure during the concerned time interval; otherwise, the structure fails during the time interval.

Step 3 : Calculate the values $\mathbf{D}\left(\bar{t}_c\right)$, namely the process ④ and ⑤ in Figure 4.

Based on the maximum failure assumption, the values $\mathbf{D}\left(\bar{t}_c\right)$ need to be calculated, and then $V\left(t_c\right)$ and $\mathbf{D}\left(\bar{t}_c\right)$ are substituted into the LSF (Eq. (7)) to calculate the extreme response, and finally one can correctly judge whether the structure is of failure or not.

Likewise, when all the discrete time instants in the entire time interval are considered, a new time vector $\bar{T}$ can be got through **Steps** 1 to 2:

$$\bar{t}_i = \max\left\{\tilde{T}_i\right\}, \ i = 1, 2, \cdots, L; \tag{11}$$

$$\bar{T} = \left[\bar{t}_1, \cdots, \bar{t}_i, \cdots, \bar{t}_L\right] \tag{12}$$

Substitute $\bar{t}_i$ into $\mathbf{D}\left(t\right)$ to obtain the decoupling values $\mathbf{D}\left(\bar{t}\right)$.

Step 4 : Through substituting $\mathbf{D}\left(\bar{t}_c\right)$ and $V\left(t_c\right)$ into the LSF (Eq. (7)), the extreme value of response $G\left(\mathbf{X}, \mathbf{D}\left(\bar{t}_c\right), V\left(t_c\right), t_c\right)$ of the structure at the time instant t_c can be captured.

After obtaining the samples of $G\left(\mathbf{X}, \mathbf{D}\left(\bar{t}_c\right), V\left(t_c\right), t_c\right)$, one can directly calculate the time-variant failure probability $P_f\left(0, t_c\right)$ such that

$$P_f\left(0, t_c\right) = \Pr\left\{G\left(\mathbf{X}, \mathbf{D}\left(\bar{t}_c\right), V\left(t_c\right), t_c\right) < 0\right\} \tag{13}$$

It should be emphasized that the proposed method is established based on two assumptions: (1) Progressive degradation assumption: the considered structure degrades at a slow rate and can be described by a deterministic progressive degradation model; (2) Maximum failure assumption: the structure fails only

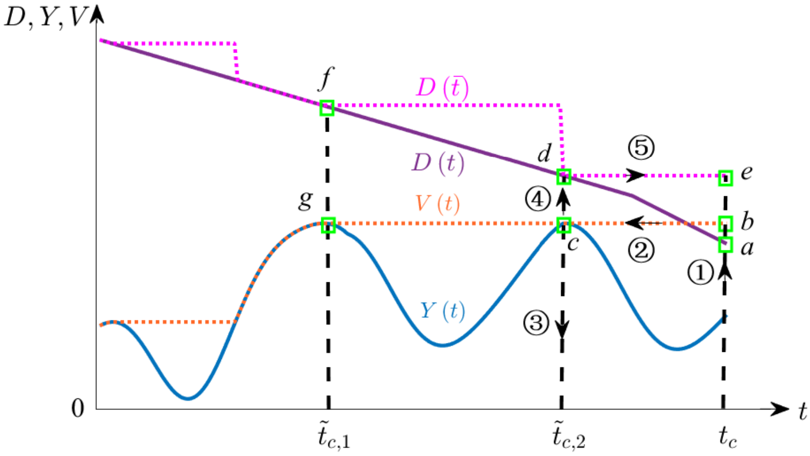

Figure 4: Schematic diagram of decoupling strategy

before the maximum load effect occurs since the first-passage problem is considered; otherwise, the structure is considered to be safe for the concerned time interval. Based on above two assumptions, we have

$$\begin{aligned} W_{\min}\left(\mathbf{X},\mathbf{D}\left(t_c\right),Y\left(t_c\right),t_c\right) &= \min_{t\in[0,t_c]}\left\{G\left(\mathbf{X},\mathbf{D}\left(t\right),Y\left(t\right),t\right)\right\} \\ &= \min_{t\in[0,t_c]}\left\{R\left(\mathbf{X},\mathbf{D}\left(t\right),t\right)-S\left(\mathbf{X},\mathbf{D}\left(t\right),Y\left(t\right),t\right)\right\} \\ &= R\left(\mathbf{X},\mathbf{D}\left(\bar{t}_c\right),t_c\right)-\max_{t\in[0,t_c]}\left\{S\left(\mathbf{X},\mathbf{D}\left(\bar{t}_c\right),Y\left(t\right),t\right)\right\} \\ &= R\left(\mathbf{X},\mathbf{D}\left(\bar{t}_c\right),t_c\right)-S\left(\mathbf{X},\mathbf{D}\left(\bar{t}_c\right),V\left(t_c\right),t_c\right) \\ &= G\left(\mathbf{X},\mathbf{D}\left(\bar{t}_c\right),V\left(t_c\right),t_c\right) \end{aligned} \tag{14}$$

the term $G\left(\mathbf{X},\mathbf{D}\left(\bar{t}_c\right),V\left(t_c\right),t_c\right)$ is actually equivalent to $W_{\min}\left(\mathbf{X},\boldsymbol{\Xi},t_c\right)$ mentioned in Eq.(5). Let us define $G\left(\mathbf{X},\mathbf{D}\left(\bar{t}_c\right),V\left(t_c\right),t_c\right)$ as the time-variant EEV-LSF for the time interval $[0,t_c]$, and denote it as $\bar{Z}=G\left(\mathbf{X},\mathbf{D}\left(\bar{t}_c\right),V\left(t_c\right),t_c\right)$. Then, the time-variant failure probability can be expressed as

$$P_f\left(0,t_c\right)=\int_{-\infty}^{0}p_{\bar{Z}}\left(\bar{z},t_c\right)\mathrm{d}\bar{z} \tag{15}$$

where $p_{\bar{Z}}\left(\bar{z},t_c\right)$ denotes the PDF of EEV-LSF at the time instant t_c. Then, the task changes to drive the PDF of EEV-LSF, i.e., $p_{\bar{Z}}\left(\bar{z},t_c\right)$. In the following section, the FEM-MEM is applied to fulfill this aim.

3.2. The FEM-MEM to reconstruct the PDF of transformed EEV-LSF

3.2.1. Box-Cox transformation

It is known that the distribution of EEV-LSF always exhibits non-normal characteristic. The tail of distribution of EEV-LSF is crucial to time-variant reliability analysis. Since the distribution of EEV-LSF with a long tail of distribution is usually quite difficult to capture with high accuracy, this paper first performs the Box-Cox transformation on EEV-LSF, where the distribution of EEV-LSF after transformation turns to be normal or weakly non-normal. Then, only the short tail of distribution is involved, whereby the failure probability can be captured with high accuracy.

As mentioned, the EEV-LSF $G(\mathbf{X}, \mathbf{D}(\bar{t}), V(t), t)$ for time-variant reliability analysis can be expressed as

$$G(\mathbf{X}, \mathbf{D}(\bar{t}), V(t), t) = R(\mathbf{X}, \mathbf{D}(\bar{t}), t) - S(\mathbf{X}, \mathbf{D}(\bar{t}), V(t), t) \tag{16}$$

where both $R(\mathbf{X}, \mathbf{D}(\bar{t}), t)$ and $S(\mathbf{X}, \mathbf{D}(\bar{t}), V(t), t)$ are always greater than 0. Consequently, based on the Box-Cox transformation [55, 56], Eq. (16) can be equivalently expressed as

$$\tilde{g}(\mathbf{X}, \mathbf{D}(\bar{t}), V(t), t) = \begin{cases} \frac{\eta(\mathbf{X}, \mathbf{D}(\bar{t}), V(t), t)^{\kappa} - 1}{\kappa}, \ \kappa \neq 0 \\ \ln\left[\eta(\mathbf{X}, \mathbf{D}(\bar{t}), V(t), t)\right], \ \kappa = 0 \end{cases} \tag{17}$$

where

$$\eta(\mathbf{X}, \mathbf{D}(\bar{t}), V(t), t) = \frac{R(\mathbf{X}, \mathbf{D}(\bar{t}), t)}{S(\mathbf{X}, \mathbf{D}(\bar{t}), V(t), t)} \tag{18}$$

and κ is the Box-Cox transformation parameter.

Note that when the Box-Cox transform is executed, the format of the LSF changes from the subtractive format originally defined in this paper to the ratio format; however, the failure domains corresponding to the LSFs of both formats are identical and do not pose any obstacle to the execution of the proposed decoupling strategy. In order to improve the accuracy for reliability analysis of EEV-LSF with highly-skewed distribution, the value of parameter κ should make the skewness $\alpha_{3\tilde{g}}$ of $\tilde{g}(\mathbf{X}, \mathbf{D}(\bar{t}), V(t), t)$ as small as possible. Since the positive skewness of $\eta(\mathbf{X}, \mathbf{D}(\bar{t}), V(t), t)$ is always involved, one can simply set the value of κ as 10^{-4} to fulfill the significant skewness reduction as a quasi-optimal option with high efficiency according to our computational experiences. It is worth stating that although the Box-Cox transform is formally close to the logarithmic transform when κ is taken as 10^{-4}, however, based on our computational experience, the Box-Cox transform is more competitive in terms of accuracy when used to calculate the failure probability compared to the direct use of the logarithmic transform.

Then, the time-variant failure probability can be expressed as

$$P_f(0, t_c) = \int_{-\infty}^{0} p_{\tilde{Z}}(\tilde{z}, t_c)\, \mathrm{d}\tilde{z} \tag{19}$$

where $\tilde{Z} = \tilde{g}(\mathbf{X}, \mathbf{D}(\bar{t}), V(t), t)$, and $p_{\tilde{Z}}(\tilde{z}, t_c)$ denotes the PDF of $\tilde{g}(\mathbf{X}, \mathbf{D}(\bar{t}), V(t), t)$ during the time interval $[0, t_c]$.

3.2.2. FEM-MEM

It is generally difficult to analytically obtain the PDF of $\tilde{g}(\mathbf{X}, \mathbf{D}(\bar{t}), V(t), t)$ for complex engineering problems. Thus, alternative simulation-based methods could be regarded as effective ways to derive the distribution. Since a large number of random variables are involved in time-variant reliability analysis, the integer moments-based maximum entropy method (IM-MEM) may not be appropriate to recover the PDF. As an extension of IM-MEM, the fractional moments (FM)-based MEM (FM-MEM) has recently received increasing attention due to its attractive features in reconstructing an unknown distribution [57, 58, 59, 60]. Although the FM-MEM overcomes the disadvantages of IM-MEM to some extent, many problems could be still encountered, which result in the difficulty of ensuring the robustness and convergence in different cases [61, 62, 63]. In that regard, the fractional exponential moments (FEM)-based MEM (FEM-MEM) is introduced to circumvent the difficulty in a robust, efficient and accurate manner [61, 62, 63].

Since different distribution domains could be involved in different problems, a coordinate transformation is first implemented such that $Z_1 = \tilde{Z}/\tilde{Z}_{\max}$ to tackle different problems in a uniform way, where $\tilde{Z}_{\max} = 1.2 \max\left\{\tilde{Z}_r\right\}$, $r = 1, 2, \cdots, N$, and $\tilde{Z}_r$'s are the sample values of $\tilde{Z}$. Then, define $U = Z_1 - Z_{1,\text{lower}}$, where $Z_{1,\text{lower}}$ denotes the lower bound of Z_1. Actually, $Z_{1,\text{lower}}$ can be approximately estimated by

$$Z_{1,\text{lower}} = \mu_{Z_1} - (5 - 2\gamma_{Z_1})\, \sigma_{Z_1} \tag{20}$$

where μ_{Z_1}, σ_{Z_1} and γ_{Z_1} are the sample mean, standard deviation and skewness of Z_1, which can be approximately estimated by the sampling technique in subsection 3.2.3. As a matter of fact, the procedures above are the normalization of arbitrary distribution range from $(-\infty, +\infty)$ to a bounded domain, where only linear translation and scale transformation are carried out.

The FEM of the variable U is usually defined as [63]

$$\mathbb{E}\left[\exp\left(-\alpha_k U\right)\right] = \int_{\Omega_U} \exp\left(-\alpha_k u\right) p_U\left(u\right) \mathrm{d}u \tag{21}$$

where α_k denotes the fractional order, Ω_U is the distribution domain of U, and $p_U\left(u\right)$ is the PDF of U. In fact, the FEM is equivalent to the moment generating function, which also contains the information about a large number of integer moments [64] and can sufficiently characterize an unknown PDF.

Then, the FEM-MEM with a total of K constraints can be formulated such that

$$\begin{cases} \text{Find}: & p_U\left(u\right) \\ \text{Maximize}: & \mathcal{H}\left[p_U\left(u\right)\right] = -\int_{\Omega_U} p_U\left(u\right) \ln\left[p_U\left(u\right)\right] \mathrm{d}u \\ \text{Constrains}: & \int_{\Omega_U} \exp\left(-\alpha_k u\right) p_U\left(u\right) \mathrm{d}u = M_U^{\alpha_k}, \quad k = 0, 1, \cdots, K \end{cases} \tag{22}$$

where $\mathcal{H}\left[p_U\left(u\right)\right]$ denotes the Shannon entropy and $M_U^{\alpha_k}, k = 1, 2, .., K$ denotes the sample FEM. The constraints mean that the analytical FEMs of U should be identical with the sampled ones. Correspondingly, the PDF $p_U\left(u\right)$ can be represented as

$$p_U\left(u\right) = \exp\left[-\lambda_0 - \sum_{k=1}^{K} \lambda_k \exp\left(-\alpha_k u\right)\right] \tag{23}$$

where

$$\lambda_0 = \ln\left\{\int_{\Omega_U} \exp\left[-\sum_{k=1}^{K} \lambda_k \exp\left(-\alpha_k u\right)\right] \mathrm{d}u\right\} \tag{24}$$

and $\boldsymbol{\lambda} = \left[\lambda_1, \lambda_2, \cdots, \lambda_K\right]^T$ is the vector collecting Lagrange multipliers. The constrained optimization above (Eqs. (22)) has been proven to be equivalent to the following unconstrained optimization problem [59]:

$$\begin{cases} \text{Find} : \boldsymbol{\lambda} = \left[\lambda_1, \lambda_2, \cdots, \lambda_K\right]^T \text{ and } \boldsymbol{\alpha} = \left[\alpha_1, \alpha_2, \cdots, \alpha_K\right]^T \\ \text{Minimize} : \mathscr{L}\left(\boldsymbol{\lambda}, \boldsymbol{\alpha}\right) = \ln\left[\int_{\Omega_U} \exp\left(-\sum_{k=1}^{K} \lambda_k \exp\left(-\alpha_k u\right)\right) \mathrm{d}u\right] + \sum_{k=1}^{K} \lambda_k M_U^{\alpha_k} \end{cases} \tag{25}$$

where $\boldsymbol{\alpha} = \left[\alpha_1, \alpha_2, \cdots, \alpha_K\right]^T$ denotes the fractional order vector. For simplicity, the simplex search method is always employed to obtain the solutions.

It has been proven in Refs. [65, 61] that when the fractional orders are adopted as $\alpha_k = k\bar{\alpha}/K, k = 1, 2, \cdots, K$, the estimated PDF $p_U(u)$ can still converge in entropy to the underlying true density. Then, we assume $\alpha_k = k\alpha^*, k = 1, 2, \cdots, K$, where α^* is the initial fractional order and $\alpha = [\alpha^*, 2\alpha^*, 3\alpha^*, \cdots, K\alpha^*]^T$. Since the low-order FEMs are always sufficient to recover the PDF, the fractional order α^* is restricted in the domain $[-2, 2]$, and the number of FEMs is specially adopted as $K = 2$ in the analysis, which can guarantee the accuracy and robustness. Then, Eq. (25) can be further expressed as

$$\begin{cases} \text{Find } : \boldsymbol{\lambda} = [\lambda_1, \lambda_2, \cdots, \lambda_K]^T \text{ and } \alpha^* \\ \text{Minimize} : \mathcal{L}(\alpha^*, \boldsymbol{\lambda}) = \ln \left[\int_{\Omega_U} \exp\left(-\sum_{k=1}^{m} \lambda_k \exp(-k\alpha^* \cdot u)\right) \mathrm{d}u \right] + \sum_{k=1}^{K} \lambda_k M_U^{k\alpha^*} \\ s.t. \ -2 \le \alpha^* \le 2 \end{cases} \tag{26}$$

which can be solved by the bounded simplex search method in Matlab. It is noted that only $K+1$ parameters, say $\boldsymbol{\lambda} = [\lambda_1, \lambda_2, \cdots, \lambda_K]^T$ and α^*, need to be specified to reconstruct the PDF $p_U(u)$. In that regard, an estimator-corrector scheme in Ref. [66] is further employed, where only the initial value of α^* needs to be provided, denoted as $\tilde{\alpha}^*$. Besides, although α^* is defined between -2 to 2, the initial value $\tilde{\alpha}^*$ should not be arbitrarily chose, which could be assigned a value according to the sample skewness of $\tilde{Z}$ $(\alpha_{3\tilde{Z}})$, i.e., $\tilde{\alpha}^* = \mathrm{sign}(\alpha_{3\tilde{z}}) \times 0.5$. Once the initial value $\tilde{\alpha}^*$ is provided, the initial fractional order vector can be determined as $\tilde{\boldsymbol{\alpha}} = [\tilde{\alpha}^*, 2\tilde{\alpha}^*, 3\tilde{\alpha}^*, \cdots, K\tilde{\alpha}^*]^T$, and the initial values of Lagrange multipliers can be promptly determined by solving a linear equation such that [66]

$$\tilde{\boldsymbol{\lambda}} = \boldsymbol{Q}^{-1}\mathbf{M}_U \tag{27}$$

where $\mathbf{M}_U = \left[M_U^{\alpha^*}, ...M_U^{k\alpha^*}, ..., M_U^{K\alpha^*}\right]^T$, $\boldsymbol{Q}[k, l] = \mathbb{E}[F_k(u) f_l'(u)]$, where $f_l(u) = \exp(-l\tilde{\alpha}^* u)$, $F_k(u) = \int_{\Omega_U} f_k(u)\, du, k, l = 1, 2, \cdots, K$. Then, $\tilde{\boldsymbol{\alpha}} = [\tilde{\alpha}^*, 2\tilde{\alpha}^*, 3\tilde{\alpha}^*, \cdots, K\tilde{\alpha}^*]^T$ and $\tilde{\boldsymbol{\lambda}} = \left[\tilde{\lambda}_1, \tilde{\lambda}_2, \cdots, \tilde{\lambda}_K\right]^T$ can be used as the initial values to further correct the solutions by Eq.(26). Once the PDF $p_U(u)$ is obtained, the PDF $p_{\tilde{Z}}(\tilde{z}, t_c)$ can be uniquely determined through the linear translation and scale transformation.

3.2.3. *Weighted sampling in high-dimension for FEMs assessment*

As mentioned, the high-dimensional probability space usually needs to be tackled in time-variant reliability analysis, where the loading stochastic process is expanded as a large number of uncorrelated random variables. It is widely recognized that the high-dimensional uncertainty quantification is still a troublesome problem, where the "curse of dimensionality" could be encountered. In other words, the existing techniques for uncertainty propagation, which are appropriate for low-dimensional cases, may fail in high-dimension. Since MCS or its variant, e.g., quasi-MCS, is irrespective of the dimension, it could be the feasible choice for FEMs assessment when the high-dimensional random inputs are considered. However, the low computational efficiency of MCS still prohibits its practical applications, especially for large-scale structures. In this paper, a weighted sampling strategy [67, 68] is employed to evaluate the FEMs with the balance of accuracy and efficiency, which is established based on the quasi-MCS and Voronoi cells.

The FEMs involved in FEM-MEM can be further expressed as

$$\begin{aligned}\mathbb{E}\left[\exp\left(-\alpha_k u\right)\right] &= \int_{\Omega_U} \exp\left(-\alpha_k u\right) p_U\left(u\right) \mathrm{d}u \\ &= \int_{\Omega_{\mathbf{X}}\times\Omega_{\boldsymbol{\Xi}}} \exp\left(-\alpha_k u\left(\mathbf{X},\boldsymbol{\Xi},t_c\right)\right) p_{\mathbf{X}}\left(\mathbf{x}\right) p_{\boldsymbol{\Xi}}\left(\boldsymbol{\xi}\right) \mathrm{d}\mathbf{x}\mathrm{d}\boldsymbol{\xi} \\ &= \int_{\Omega_{\tilde{\boldsymbol{\Xi}}}\times\Omega_{\boldsymbol{\Xi}}} \exp\left(-\alpha_k u\left(N^{-1}\left[\tilde{\boldsymbol{\Xi}}\right],\boldsymbol{\Xi},t_c\right)\right) p_{\tilde{\boldsymbol{\Xi}}}\left(\tilde{\boldsymbol{\xi}}\right) p_{\boldsymbol{\Xi}}\left(\boldsymbol{\xi}\right) \mathrm{d}\tilde{\boldsymbol{\xi}}\mathrm{d}\boldsymbol{\xi} \\ &= \int_{\Omega_{\boldsymbol{\Theta}}} \exp\left(-\alpha_k u\left(\boldsymbol{\Theta},t_c\right)\right) p_{\boldsymbol{\Theta}}\left(\boldsymbol{\theta}\right) \mathrm{d}\boldsymbol{\theta}\end{aligned} \tag{28}$$

where N^{-1} denotes the inverse Nataf transformation, which converts the non-normal random vector $\mathbf{X}$ to be the independent standard normal one $\tilde{\boldsymbol{\Xi}}$, whose joint PDF is $p_{\tilde{\boldsymbol{\Xi}}}\left(\tilde{\boldsymbol{\xi}}\right)$; $\Omega_{\mathbf{X}}\times\Omega_{\boldsymbol{\Xi}}$ denotes the joint distribution domain of $\mathbf{X}$ and $\boldsymbol{\Xi}$, and $\boldsymbol{\Theta}=\left[\boldsymbol{\Xi},\tilde{\boldsymbol{\Xi}}\right]=\left[\Theta_1,\Theta_2,\cdots,\Theta_d,\cdots,\Theta_D\right]\left(D=d+M\right)$ represents the independent standard normal random vector.

In that regard, only the D-dimensional standard normal space needs to be tackled. In this paper, a weighted sampling strategy is employed (see Appendix A), where the points and weights are generated in the D-dimensional standard normal space for numerical assessment of FEMs such that

$$\mathbb{E}\left[\exp\left(-\alpha_k u\right)\right] = \sum_{r=1}^{N} \omega_r \exp\left(-\alpha_k u\left(\boldsymbol{\theta}_r,t_c\right)\right) \tag{29}$$

where ω_r and $\boldsymbol{\theta}_r$, $r=1,2,\cdots,N$, are the weights and points in standard normal space and N is the total number of points.

According to our computational experiences, a total of 400 samples could be sufficient for time-variant reliability analysis for explicit LSFs with high accuracy, while a total of 1000 samples coule be necessary to achieve highly accurate results for implicit LSFs.

4. Numerical Examples

In this section, three classical numerical examples are investigated to verify the accuracy and efficiency of the proposed method for time-variant reliability evaluations, where the computational results by MCS and PHI2 [15] are also provided for comparisons. The PHI2 method is performed by UQLab [69], a Matlab-based software framework. Besides, it should be pointed out that the conventional EVD-based approach is applied in MCS, where the double-loop computations are implemented.

4.1. Example 1: Corroded steel beam

First, a simply supported steel beam with a rectangular cross section subjected to a time-variant pinpoint load $F(t)$ at the mid span is considered [15], as shown in Figure 5. The length of the beam is $L = 5\text{m}$. Due to the corrosion of steel beam, the sizes of the cross section $b(t)$ and $h(t)$ decrease monotonically with time such that

$$b(t) = b_0 - 2kt; \quad h(t) = h_0 - 2kt; \tag{30}$$

where b_0 and h_0 are the initial width and height of the beam and $k = 0.03\text{mm/year}$.

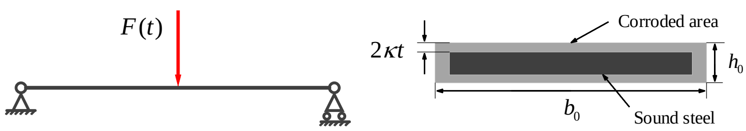

Figure 5: Corroded beam under a midspan load

The bending failure is considered, where the time-variant LSF is expressed as [15]

$$Z(t) = G(\mathbf{X}, Y(t), t) = \frac{b(t)\, h^2(t)\, \sigma_y}{4} - \left(\frac{F(t)\, L}{4} + \frac{\rho_{st} b_0 h_0 L^2}{8} \right) \tag{31}$$

where $\rho_{st} = 78.5\text{kN/m}^3$ is the steel mass density. Besides, the distributions of input random variables and loading stochastic process are gathered in Table 1.

Table 1: Probabilistic information for corroded steel beam

Paramter	Description	Distribution	Mean	COV
σ_y	Steel yielding stress	Lognormal	180 MPa	0.10
b_0	Width of the beam	Lognormal	0.2 m	0.05
h_0	Height of the beam	Lognormal	0.04 m	0.10
$F(t)$	Concentrated load	Gaussian process	3500 N	0.20

Note: COV = Coefficient of variation.

In this example, the load $F(t)$ is assumed to be a stationary Gaussian process, where the autocorrelation coefficient function takes

$$\rho(t_1, t_2) = \exp\left(-\left(\frac{t_2 - t_1}{2}\right)^2\right) \tag{32}$$

The EOLE expansion is first employed to discretize the loading stochastic process $F(t)$ as a time-variant function of independent standard normal variables. The truncated number is specified as $M = 22$ in this example. The failure probability in the time duration $[0, 30]$ year is of first concern and the time duration is uniformly divided into 200 intervals with 201 time instants. The total number of random variables in this example is 25, where a total of 400 weighted samples are selected in the 25-dimensional independent standard normal space. Correspondingly, a total of 400 deterministic model evaluations are carried out to obtain the failure probability at the end of the life-time of the structure ("right-boundary problem") [70].

For the 30th year, that is $t_c = T = 30$th, the initial fractional order $\tilde{\alpha}^*$ is -0.5, where $\alpha_{3\tilde{Z}} = -0.0781$. Accordingly, the initial Lagrangian multipliers are $\tilde{\boldsymbol{\lambda}} = [-90.4380, 28.9707]^T$. The values of $\tilde{\alpha}^*$ and $\boldsymbol{\lambda}$ at other discrete time points can be similarly obtained. For the sake of brevity, the relevant data are not reported.

Figure 6 plots the PDF and cumulative distribution function (CDF) (logarithmic scale) of transformed EEV-LSF when $t_c = T = 30$th year by the proposed method, where the histogram and CDF curve by MCS ($= 2.01 \times 10^8$ runs) are provided for comparisons. It is known that the MCS-based time-variant reliability method needs to perform a large number of LSF evaluations at each discrete time instant [45]. Herein, a total of 1×10^6 LSF calls at each discrete time instant is employed. Since a total of 201 time instants are involved, the total number of LSF calls by MCS is $201 \times 1 \times 10^6 = 2.01 \times 10^8$ to get the distribution of transformed EEV-LSF and failure probability at the 30th year. It is clear that the results estimated by the proposed method agree very well with those by MCS, demonstrating the accuracy of the proposed method for evaluating the PDF of transformed EEV-LSF. The reliability index at the 30th year obtained from the proposed method is 2.3681, which is close to 2.3212 obtained from MCS. Similarly, Figure 7 shows the comparisons of CDFs in logarithmic scale at the 15th, 20th and 25th years, respectively, by the proposed method and MCS. Clearly, the results obtained from the proposed method always accord well with those by MCS. In addition, the reliability indexes at the these three years calculated by the proposed method are 2.6208, 2.5337 and 2.4076, where the corresponding reliability indexes by MCS are 2.6431, 2.5270 and 2.4185.

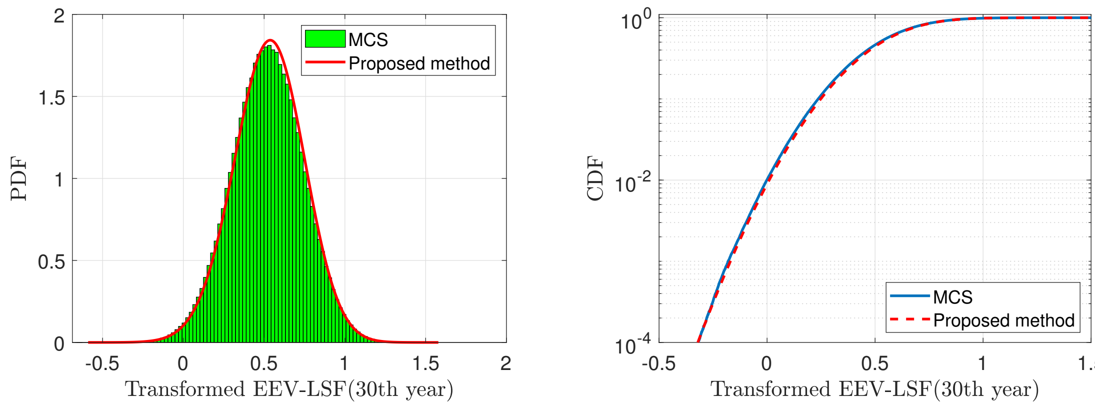

(a) PDF (b) CDF

Figure 6: PDF and CDF of transformed EEV-LSF at the 30th year for the corroded steel beam.

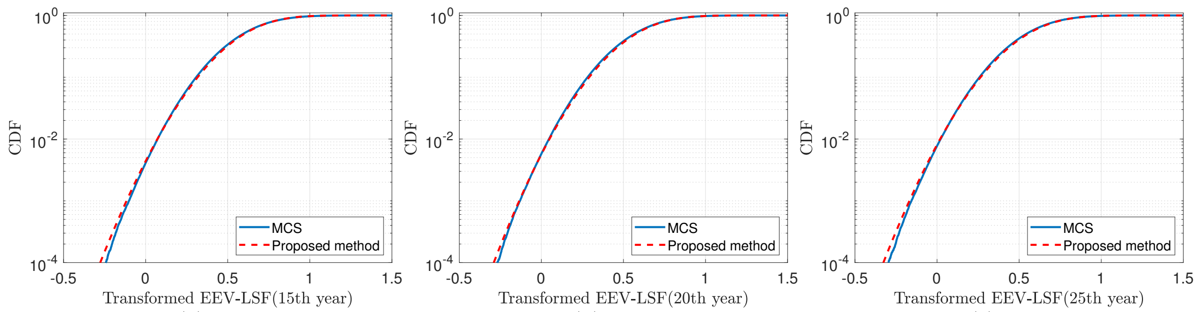

(a) (b) (c)

Figure 7: CDFs at three different years for the corroded steel beam.

The PDF surface of transformed EEV-LSF over the time interval $[0, 30]$ year is computed and plotted in Figure 8 (a). The time-variant failure probabilities are depicted in Figure 8 (b), which are also listed in Table 2. The results by MCS and PHI2 are also given in Table 2 for comparisons, where the COVs of failure probabilities by MCS are also reported. In addition, since the quasi-MCS (e.g., Sobol sequence), which is a deterministic point set, is applied as the basic point set in the proposed method, the sampling points do not exhibit variability during different simulation runs. In that regard, the COVs of results by the proposed method are all zero. The PHI2 method is performed by UQLab, where the total number of simulations in PHI2 is 20181. If the number of LSF calls is used to measure the efficiency, the proposed method is much more efficient since only 400 calculations are required. In addition, it is clear that the results by the proposed method are obviously closer to those by MCS than those by PHI2 method in this example, where the relative errors are much smaller. The computational results above demonstrate the proposed method can accurately access the time-variant reliability indexes with high efficiency.

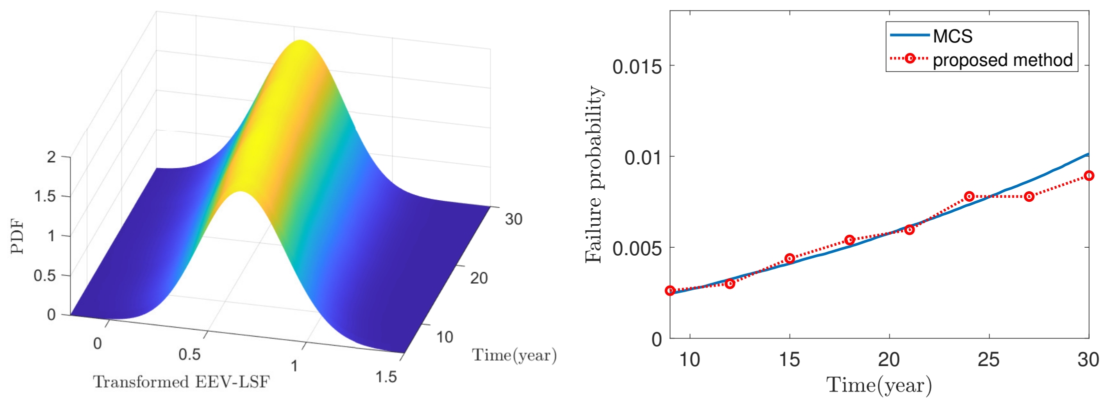

(a) PDF evolution (b) Failure probability

Figure 8: Time-variant reliability evaluation for the corroded steel beam.

To further verify the proposed method for small failure probability problems, the mean of yield strength σ_y is modified as 218MPa. The failure probabilities at the 30th year obtained by MCS and the proposed method are 7.90×10^{-4} and 7.36×10^{-4} respectively, which also shows that the proposed method can still maintain acceptable accuracy when the small failure probability is of concern. It should be emphasized that the 10^{-4}-level failure probability can be treated as a "small" failure probability problem [71, 72] in engineering practice. The failure probability smaller than 10^{-4}-level e.g., 10^{-7}-level, is usually associated with extremely rare event, considered only in some very important structures and infrastructures, and is not concerned in this paper.

Table 2: Comparisons of time-variant failure probabilities for the corroded beam

Time interval(year)	[0,9]	[0,12]	[0,15]	[0,18]	[0,21]	[0,24]	[0,27]	[0,30]
MCS ($\times 10^{-3}$)	2.45	3.24	4.11	5.04	6.16	7.34	8.64	10.14
(COV) (%)	(2.02)	(1.75)	(1.56)	(1.40)	(1.27)	(1.16)	(1.07)	(0.99)
PHI2 ($\times 10^{-3}$)	2.67	3.88	5.30	6.97	8.91	11.17	13.79	16.83
(R.E.) (%)	(8.83)	(19.67)	(29.06)	(38.16)	(44.68)	(52.10)	(59.67)	(66.00)
Proposed method ($\times 10^{-3}$)	2.62	3.00	4.39	5.40	5.97	7.80	7.79	8.94
(R.E.) (%)	(6.83)	(7.54)	(6.78)	(7.14)	(3.12)	(6.19)	(9.83)	(11.81)

Note: R.E. = Relative error.

4.2. Example 2: Cantilever tube structure

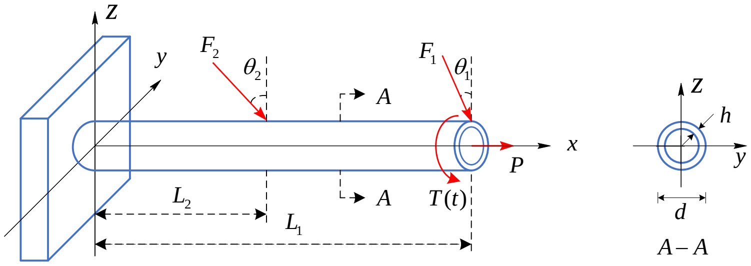

Figure 9: A cantilever tube structure

The second example considers a cantilever tube structure, as shown in Figure 9 [45]. Three random external forces F_1, F_2, P and a torque random process $T(t)$ are applied to the structure. A loss of yield strength due to the material degradation is considered, where a linearly decreasing time-variant function $R(t) = R_0(1 - 0.01t)$ is used to describe this process and R_0 stands for the initial yield stress.

In this example, the structure fails when the maximum Von-Mises stress $\sigma_{\max}$ at the end of the tube exceeds its time-variant bearing capacity, i.e., $R(t)$, over a time period of 5 years:

$$Z(t) = G(\mathbf{X}, Y(t), t) = R(t) - \sigma_{\max}(t) \tag{33}$$

where

$$\sigma_{\max}(t) = \sqrt{\sigma_x^2(t) + 3\tau_{zx}^2(t)} \tag{34}$$

$$\sigma_x(t) = \frac{F_1(t)\sin(\theta_1) + F_2\sin(\theta_2) + P}{A} + \frac{M(T)d}{2I} \tag{35}$$

$$M(t) = F_1(t)\cos(\theta_1)L_1 + F_2\cos(\theta_2)L_2 \tag{36}$$

$$A = \frac{\pi}{4}[d^2 - (d - 2h)^2] \tag{37}$$

$$I = \frac{\pi}{64}[d^4 - (d - 2h)^4] \tag{38}$$

$$\tau_{zx}(t) = \frac{T(t)d}{4I} \tag{39}$$

and $T(t)$ is a stationary Gaussian process whose autocorrelation function is $\rho(t_1, t_2) = \exp(-(\frac{t_2 - t_1}{0.5})^2)$. The distributions of other parameters involved in this example are listed in Table 3.

Table 3: Distribution of parameters for the cantilever tube

variable	Distribution	Mean	COV
$T(t)$	Gaussian process	1700 N · m	0.10
F_1	Normal	1800 N	0.10
F_2	Normal	1800 N	0.10
P	Lognormal	1000 N	0.10
h	Normal	5 mm	0.019
d	Normal	42 mm	0.02
R_0	Normal	500 MPa	0.10
θ_1	Deterministic	5°	0
θ_2	Deterministic	10°	0
L_1	Deterministic	120 mm	0
L_2	Deterministic	60 mm	0

First, the loading stochastic process $T(t)$ is discretized by EOLE, where the truncated number $M = 15$ is determined accordingly. In this regard, this example involves a total of 21 random variables in both structural parameters and external excitations. Similarly, a total of 400 weighted samples are determined in this 21-dimensional probability space by the proposed method, indicating 400 repeatedly deterministic model evaluations are required in the proposed method. The time interval [0,5] year is considered and discretized into 200 time intervals with 201 time instants, where $\Delta t = 0.3$ month.

For the last time point $t_c = T = 5$th, the initial fractional order $\tilde{\alpha}^*$ is -0.5, and the initial Lagrangian multipliers are $\tilde{\boldsymbol{\lambda}} = [-104.5302, 34.8236]^T$. The PDF and CDF (in logarithmic scale) of transformed EEV-LSF when $t_c = T = 5$th year are evaluated by the proposed method and plotted in Figure 10, where the results by MCS ($= 2.01 \times 10^8$ runs) are also provided for comparisons. Again, it can be observed that the proposed

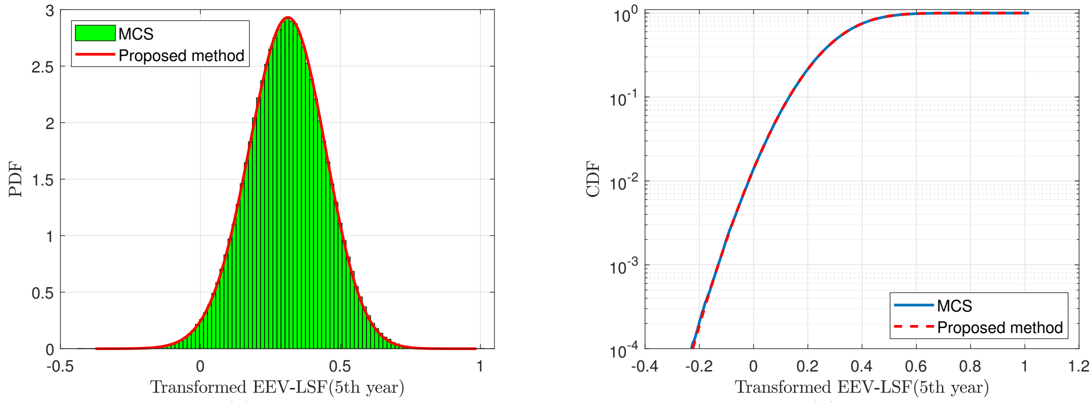

(a) PDF (b) CDF

Figure 10: PDF and CDF of transformed EEV-LSF at the 5th year for the cantilever tube.

method can provide accurate estimation for the PDF of transformed EEV-LSF within the time interval [0,5] year. The reliability indexes at the 5th year given by the proposed method and MCS are 2.1998 and 2.2004, respectively, which are very close to each other.

Figure 11 depicts the comparisons of CDFs in logarithmic scale at three different years, say the 2nd, 3rd, and 4th years. Note that the CDFs evaluated by the proposed method are still in close agreements with those by MCS, demonstrating the accuracy of the proposed method for deriving the distributions related to time-variant reliability analysis. The reliability indexes at these three years evaluated by the proposed method are 2.5062, 2.3666 and 2.2691, where the comparative results by MCS are 2.5345, 2.4012 and 2.2954. It is clear that the results by the proposed method also accord pretty well with those by MCS.

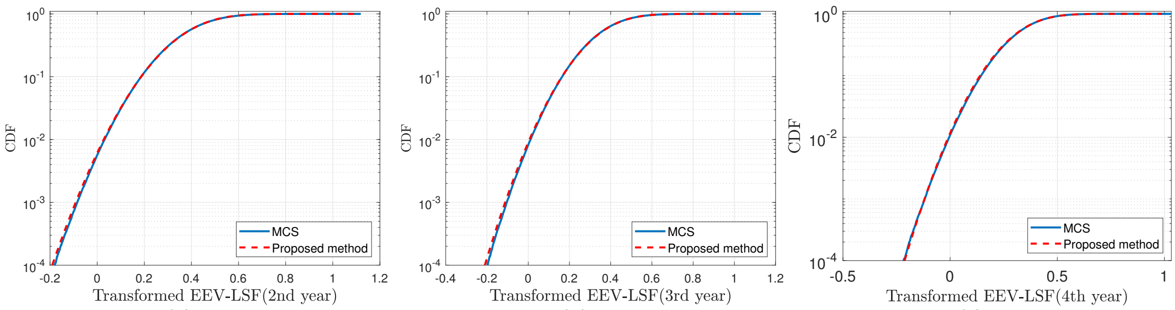

(a) (b) (c)

Figure 11: CDFs at three different years for the cantilever tube.

Similarly, the PDF surface of transformed EEV-LSF over the time interval $[0, 5]$ year is plotted in Figure 12 (a), whereas the failure probabilities are compared in Figure 12 (b), respectively. It is seen that the proposed method provides a fine estimation for the evolution of failure probabilities in different time intervals. Table 4 lists the time-variant failure probabilities by the proposed method and MCS, where the COVs of failure probabilities by MCS are reported. Meanwhile, the time-variant failure probabilities results based on PHI2 are also listed in Table 4 for comparisons. The relative errors of failure probabilities by the proposed method and PHI2 are compared. It is clear that the MCS and PHI2 need to perform 2.01×10^8 and 20100 LSF calculations respectively to get the failure probability at the 5th year, while only 400 model evaluations are sufficient in the proposed method. Moreover, for this example, the results by the proposed method are obviously closer to the results by MCS than those by PHI2 again. Clearly, the proposed method can yield fairly accurate time-variant reliability with efficiency, which again validates the efficacy of the proposed method.

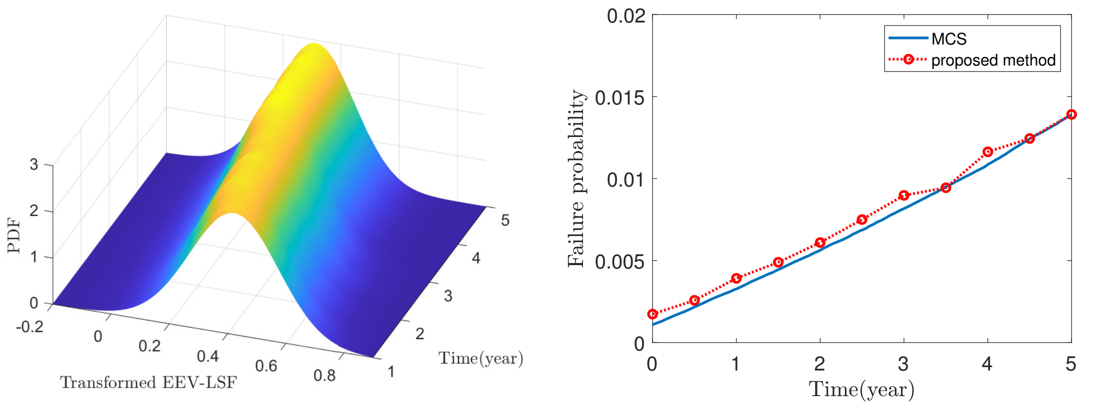

(a) PDF evalution (b) Failure probability

Figure 12: Time-variant reliability for the cantilever tube.

Table 4: Comparisons of time-variant failure probabilities for the cantilever tube

Time interval(year)	[0,3.3]	[0,3.6]	[0,3.9]	[0,4.2]	[0,4.5]	[0,4.8]	[0,5]
MCS ($\times 10^{-2}$)	0.90	0.98	1.06	1.14	1.24	1.33	1.39
(COV) (%)	(1.05)	(1.00)	(0.97)	(0.93)	(0.89)	(0.86)	(0.84)
PHI2 ($\times 10^{-2}$)	1.00	1.13	1.26	1.40	1.55	1.70	1.81
(R.E.) (%)	(11.65)	(15.26)	(19.18)	(22.14)	(24.56)	(28.42)	(30.57)
Proposed method ($\times 10^{-2}$)	0.95	0.99	1.12	1.21	1.24	1.36	1.39
(R.E.) (%)	(6.50)	(1.23)	(6.52)	(5.96)	(0.20)	(2.37)	(0.15)

4.3. Example 3: A 13-storey RC frame-shear wall structure

To further check the effectiveness of the proposed method for practical complex engineering structures, a 13-storey high-rise frame-shear wall structure is considered, as shown in Figure 13 [73]. The finite-element model is built by OpenSEES software. The structure is subjected to gravity loads as well as lateral loads. The structural properties will experience degradation due to corrosion, and the lateral loads are time-variant.

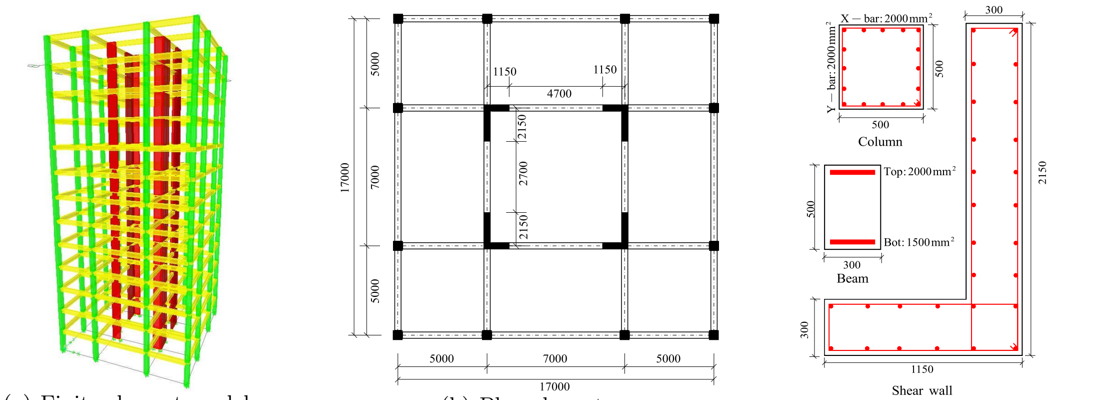

(a) Finite element model (b) Plane layout (c) Geometric size and reinforcement

Figure 13: Structural information [3]

It is recognized that the time-variant deterioration of reinforced concrete members is related to both the concrete and steel materials as well as other chemical or physical quantities [74]. Therefore, in this example, the compressive strength of concrete and the yield strength of reinforcement are considered to be random quantities, which vary against time with the following relationships [3]:

$$f_{pc}(t) = f_{pc,0}\left(10 - 8 \times 10^{-7} t^3\right) \tag{40}$$

$$f_y(t) = f_{y,0}\left(1 - 2.2 \times 10^{-6} t^3\right) \tag{41}$$

where $f_{pc,0}$ is the compressive strength of concrete at the initial time; and $f_{y,0}$ is the yield strength of reinforcement at the initial time. The uniaxial nonlinear constitutive models of concrete and reinforcement are shown in Figure 14 [73].

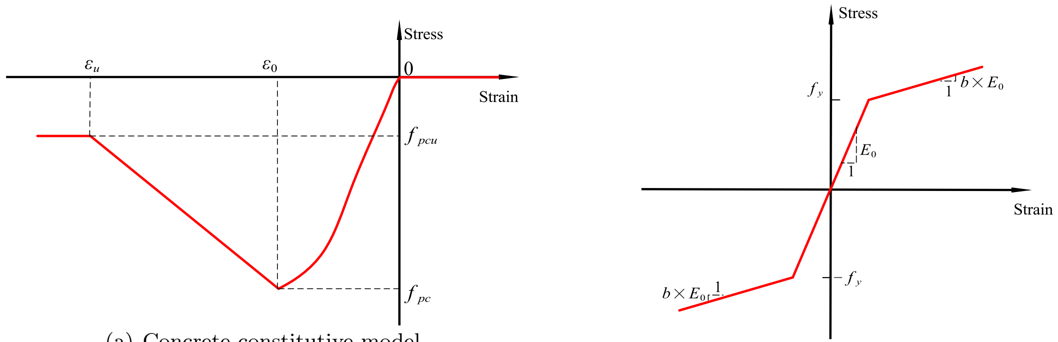

(a) Concrete constitutive model

(b) Steel constitutive model

Figure 14: Uniaxial constitutive models

In addition, the total lateral force $F(t)$ applied to the structure is assumed to be a stationary Gaussian process, where the autocorrelation coefficient function takes

$$\rho(t_1, t_2) = \exp\left(-\left(\frac{t_2 - t_1}{4}\right)^2\right) \tag{42}$$

and the lateral force applied to each storey is [73]:

$$F_i(t) = \frac{M_i h_i^{\zeta}}{\sum_{j=1}^{13} M_j h_j} F(t) \tag{43}$$

where M_i, h_i and $F_i(t)$ are the mass, height and applied force of the ith storey of the structure and $\zeta = 1.3$ is the correction factor of height.

In this example, the structure is considered over 50 years and is out of service when the top displacement of the structure in the direction of lateral load, denoted as $\nu_R(t)$, is larger than the prescribed threshold $\bar{\nu}_R = 105$mm, where the time-variant LSF can be expressed as

$$Z(t) = G(\mathbf{X}, Y(t), t) = \bar{\nu}_R - |\nu_R(t)| \tag{44}$$

The probabilistic and deterministic parameters involved in this example are listed in Table 5.

A similar procedure is implemented for time-variant reliability analysis of this complex frame-shear wall structure. First, the loading stochastic process $F(t)$ is reconstructed by EOLE, where 20 independent standard normal random variables are involved. The loading stochastic process $F(t)$ is discretized into 200 time intervals with 201 time instants. Considering the randomness in structural properties, a total of 22

Table 5: Parameters for the 13-storey frame-shear wall structure

variable	Distribution	Mean	COV
$f_{pc,0}$	Normal	40 MPa	0.10
$f_{y,0}$	Normal	386 MPa	0.08
$F(t)$	Gaussian process	1.5×10^3 kN	0.20
f_{pcu}	Deterministic	10 MPa	0
ε_0	Deterministic	0.0015	0
ε_u	Deterministic	0.006	0
E_0	Deterministic	2.0×10^5 MPa	0
b	Deterministic	0.01	0

independent random variables are involved in this problem. The proposed method is then applied to analyze the time-variant reliability, where a total of 1000 weighted samples are selected in this high-dimensional probability space. For the last time point $t_c = T = 50$th, the initial fractional order $\tilde{\alpha}^*$ is -0.5, and the initial Lagrangian multipliers are determined as $\tilde{\boldsymbol{\lambda}} = [-92.8571, 29.7863]^T$.

Likewise, the PDF and CDF in logarithmic scale of transformed EEV-LSF when $t_c = T$ =50th year are estimated by the proposed method, which are shown in Figure 15. The results by MCS ($= 2.01 \times 10^6$ runs) are also provided for comparisons. Obviously, the PDF and CDF of transformed EEV-LSF still accord very well with those by MCS, which indicates the accuracy of the proposed method for deriving the whole PDF of transformed EEV-LSF. The reliability index provided by the proposed method at the 50th year is 1.84, which is almost the same with that obtained by MCS. Figure 16 plots the CDFs of transformed EEV-LSF when t_c =20th, 30th and 40th years, which are evaluated by the proposed method, and the results by MCS are also pictured as references. The results show that the proposed method still can yield accurate CDFs of transformed EEV-LSF at different years. The reliability indexes by the proposed method at these three years are 2.28, 2.13 and 2.00, respectively, where the corresponding results by MCS are 2.26, 2.12 and 1.97. Again, the accuracy of the proposed method for time-variant reliability analysis of a complex engineering structure is validated.

Figure 17 shows the evolutionary PDFs of transformed EEV-LSF and the corresponding time-variant failure probabilities. Table 6 lists the comparisons of time-variant failure probabilities at these years. Since this example involves complex finite element calculations, which means that the MCS method inevitably requires huge computation efforts, only 1×10^4 samples are used at each time instant to calculate the failure

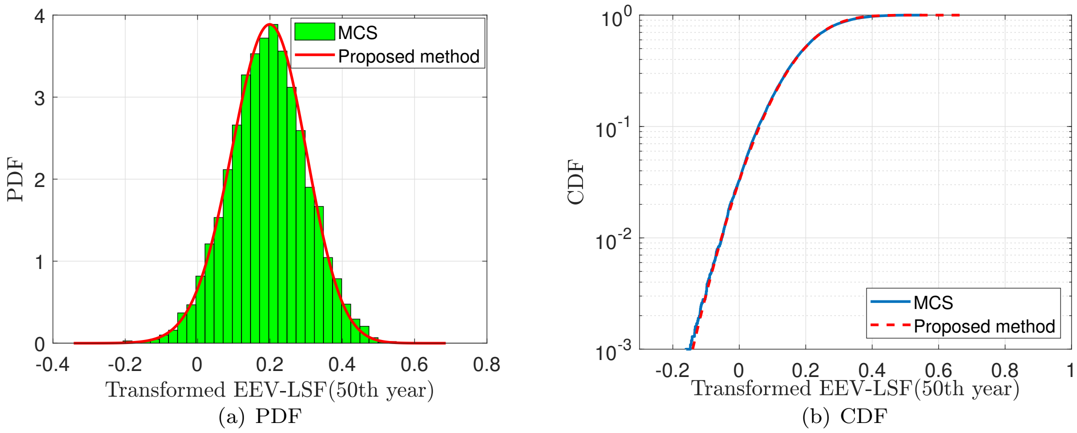

Figure 15: PDF and CDF of transformed EEV-LSF at the 50th year for the frame-shear wall structure.

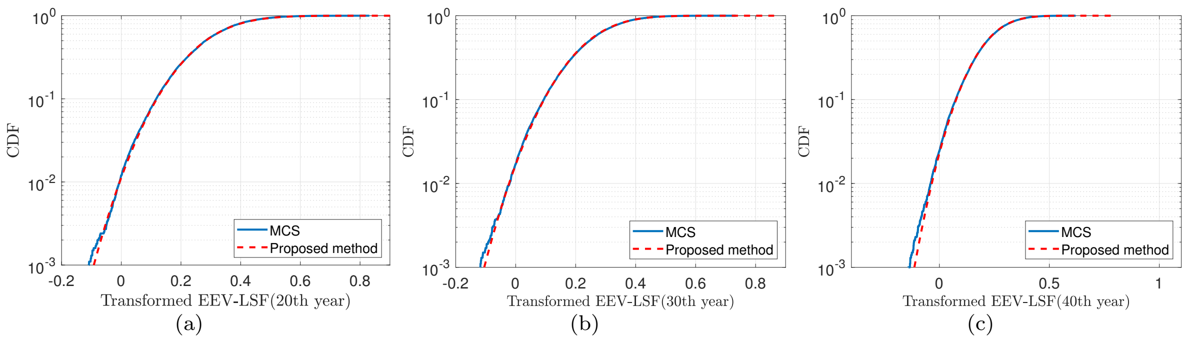

Figure 16: CDFs at three different years for the frame-shear wall structure.

probability. In that regard, the COVs of failure probabilities calculated by MCS are relatively large as shown in Table 6. In addition, both the MCS and PHI2 need to perform 2.01×10^6 calculations to get the failure probability at the 50th year, while the proposed method only needs 1000 model evaluations. Furthermore, the accuracy of time-variant failure probabilities/reliability indexes by the proposed method is obviously much better than those by PHI2 again in this example, which verifies the effectiveness of the proposed method for time-variant reliability assessment even when an implicit complex LSF with high-dimensional random inputs is considered.

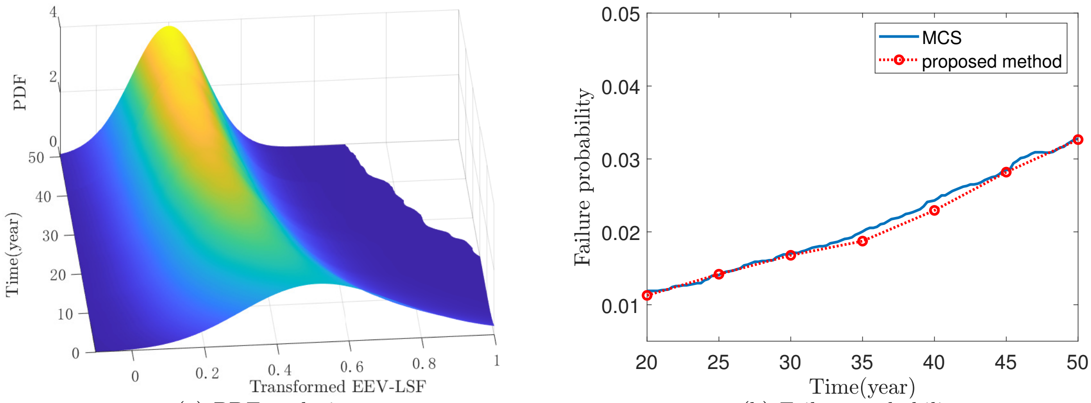

(a) PDF evolution (b) Failure probability

Figure 17: Time-variant reliability evaluation for the frame-shear wall structure.

Table 6: Comparisons of time-variant failure probabilities for the frame-shear wall structure

Time interval(year)	[0,20]	[0,25]	[0,30]	[0,35]	[0,40]	[0,45]	[0,50]
MCS ($\times 10^{-2}$)	1.19	1.40	1.70	2.00	2.43	2.84	3.27
(COV) (%)	(9.11)	(8.39)	(7.60)	(7.00)	(6.34)	(5.85)	(5.44)
PHI2 ($\times 10^{-2}$)	1.38	1.70	2.06	2.40	2.86	3.33	3.79
(R.E.) (%)	(14.19)	(21.28)	(21.02)	(19.95)	(17.60)	(17.37)	(15.81)
Proposed method ($\times 10^{-2}$)	1.13	-1.34	1.68	1.87	2.29	2.82	3.27
(R.E.) (%)	(5.15)	(0.89)	(1.26)	(6.34)	(5.59)	(0.73)	(0.14)

5. Concluding remarks

In this paper, a single-loop method is proposed for time-variant reliability analysis of structures with efficiency and accuracy. The proposed method is established based on a decoupling strategy and probability distribution reconstruction. In this method, the input loading stochastic process is first discretized into a large number of random variables by EOLE. A weighted sampling strategy is then employed to determine the sampling points and weights for model evaluations. Then, the decoupling strategy of loading stochastic process and degradation processes of structural resistance is implemented. In this strategy, the maximal value process of loading stochastic process and decoupled degradation processes during a specified time duration are extracted to determine the extreme value of load effect. Meanwhile, the corresponding degradation values of structural resistance are determined accordingly. Then, only a single-round of model evaluations are necessary to derive the required PDF for time-variant reliability analysis. The FEM-MEM is employed for the PDF derivation with efficiency and accuracy, in which the Box-Cox transformation is performed to ensure the robustness. Three numerical examples including a complex real-world case are investigated to check the effectiveness of the proposed method for time-variant reliability analysis. In all these examples, the PDF at a specified time instant can be reconstructed with accuracy and high efficiency, where only a small number of weighted samples are required. The time-variant failure probabilities can be also evaluated by the proposed method with satisfactory accuracy. The results demonstrate that the proposed method is effective for time-variant reliability analysis, where the trade-off of accuracy and efficiency can be achieved.

Acknowledgments:

The National Natural Science Foundation of China (No. 51978253) and the Fundamental Research Funds for the Central Universities (No. 531107040024) are gratefully appreciated for the financial support of this research.

Conflict of interest:

The authors declare that they have no known competing financial interests or personal relationships that could have appeared to influence the work reported in this paper.

Data Availability Statement:

Some or all data, models, or code that support the findings of this study are available from the corresponding author upon reasonable request.

Appendix A. Weighted sampling method [67]

First, a uniform point set is scattered in the unit hypercube $[0,1]^D$ by quasi-MCS (e.g., Sobol sequence) due to its low discrepancy, which is denoted as $\mathcal{P}_u = \{\mathbf{v}_r = [v_{1,r}, v_{2,r}, \cdots, v_{D,r}], r = 1, 2, \cdots, N\}$. Then, the uniform point set $\mathcal{P}_u$ is transformed into the standard normal space by using the isoprobabilistic transformation such that

$$\theta_{i,r} = \Phi^{-1}\left(F_{v_i}\left(v_{i,r}\right)\right), \ i = 1, 2, \cdots, D, \ r = 1, 2, \cdots, N \tag{A.1}$$

where Φ^{-1} denotes the inverse CDF of a standard normal distribution; and $F_{v_i}(\cdot)$ is the CDF of V_r. The transformed point set is denoted as $\mathcal{P}_t = \{\boldsymbol{\theta}_r = [\theta_{1,r}, \theta_{2,r}, \cdots, \theta_{D,r}],\ r = 1, 2, \cdots, N\}$.

Next, the input D-dimensional standard normal space could be partitioned as a set of non-overlapping subdomains by using the Voronoi cells V_r's , defined as [75]

$$V_r = \{\boldsymbol{\theta} \in \mathbb{R}^s, \|\boldsymbol{\theta} - \boldsymbol{\theta}_r\| \leq \|\boldsymbol{\theta} - \boldsymbol{\theta}_q\|,\ \text{for all } r \neq q\} \tag{A.2}$$

where $\boldsymbol{\theta}_r$ and $\boldsymbol{\theta}_q$ denote the different sampling points in sub-domains V_r and V_q, where $V_r \cap V_q = \varnothing$ for $r \neq q$ and $\bigcup_{r=1}^{N} V_r = \Omega_{\boldsymbol{\Theta}}$.

The weight for each Voronoi cell can be computed by covering the joint PDF $p_{\boldsymbol{\Theta}}(\boldsymbol{\theta})$ over the distribution domain such that

$$\omega_r = \int_{V_r} p_{\boldsymbol{\Theta}}(\boldsymbol{\theta})\, \mathrm{d}\boldsymbol{\theta} \tag{A.3}$$

It is clear that the weights ω_r's, $r = 1, 2, \cdots, N$, are unequal since the Voronoi cells are different with each other and are polygons. Practically, analytical computation of weights is always unfeasible, and an auxiliary MCS with a large number of samples could be implemented to compute the weights, where only the standard normal space is involved. The random samples generated by the auxiliary MCS are denoted as $\mathcal{P}_{\text{mcs}} = \left\{\tilde{\boldsymbol{\theta}}_j = \left[\tilde{\theta}_{1,j}, \tilde{\theta}_{2,j}, \cdots, \tilde{\theta}_{D,j}\right], j = 1, 2, \cdots, N_{\text{mcs}}\right\}$, where $N_{\text{mcs}} \gg N$ is the number of the auxiliary MCS samples. Usually, $N_{\text{mcs}} = 10^7 \sim 10^8$ is employed. Since this step also dose not requires the deterministic LSF calls, the computational time could be ignored compared with the time-demanding model evaluations. Then, the weights can be expressed as

$$\omega_r = \int_{V_r} p_{\boldsymbol{\Theta}}(\boldsymbol{\theta})\, \mathrm{d}\boldsymbol{\theta} \approx \frac{n_r}{N_{\text{mcs}}} \tag{A.4}$$

where n_r denotes the number of the auxiliary MCS samples located in the Voronoi cell V_r. Clearly, $\sum_{r=1}^{N} \omega_r = 1$.

To make the point set more consistent with the standard normal distributions, rearranging the points is further implemented such that [67]

$$\theta'_{i,r} = \Phi^{-1}\left(\sum_{r=1}^{N} \left(\omega_r \cdot I\left(\theta_{i,r} < \theta_{i,q}\right)\right) + \frac{1}{2}\omega_q\right) \tag{A.5}$$

where the point set $\mathcal{P}_{\text{final}} = \left\{\boldsymbol{\theta}_r' = \left[\theta_{1,r}', \theta_{2,r}', \cdots, \theta_{D,r}'\right], r = 1, 2, \cdots, N\right\}$ is taken as the final point set.

In that regard, the FEMs in Eq. (29) can be computed by

$$\mathbb{E}\left[\exp\left(-\alpha_k u\right)\right] = \sum_{r=1}^{N} \omega_r \exp\left(-\alpha_k u\left(\boldsymbol{\theta}_r', t\right)\right) \tag{A.6}$$

References

[1] C. Wang, Q. Li, B. R. Ellingwood, Time-dependent reliability of ageing structures: an approximate approach, Structure and Infrastructure Engineering 12 (2016) 1566–1572.

[2] C. Wang, H. Zhang, M. Beer, Structural time-dependent reliability assessment with new power spectral density function, Journal of Structural Engineering 145 (2019) 04019163.

[3] Z. Wan, J. Chen, J. Li, H. S. Ang, An efficient new pdem-com based approach for time-variant reliability assessment of structures with monotonically deteriorating materials, Structural Safety 82 (2020) 101878.1–101878.10.

[4] C. Jiang, T. Fang, Z. Wang, X. Wei, Z. Huang, A general solution framework for time-variant reliability based design optimization, Computer Methods in Applied Mechanics and Engineering 323 (2017) 330–352.

[5] C. Gong, D. M. Frangopol, An efficient time-dependent reliability method, Structural Safety 81 (2019) 101864.

[6] T. Zafar, Y. Zhang, Z. Wang, An efficient kriging based method for time-dependent reliability based robust design optimization via evolutionary algorithm, Computer Methods in Applied Mechanics and Engineering 372 (2020) 113386.

[7] Y. Shi, Z. Lu, Z. Huang, L. Xu, R. He, Advanced solution strategies for time-dependent reliability based design optimization, Computer Methods in Applied Mechanics and Engineering 364 (2020) 112916.

[8] Z. Meng, J. Zhao, C. Jiang, An efficient semi-analytical extreme value method for time-variant reliability analysis, Structural and Multidisciplinary Optimization 64 (2021) 1469–1480.

[9] D. Wang, H. Qiu, L. Gao, C. Jiang, A single-loop kriging coupled with subset simulation for time-dependent reliability analysis, Reliability Engineering & System Safety 216 (2021) 107931.

[10] R. Cao, Z. Sun, J. Wang, F. Guo, A single-loop reliability analysis strategy for time-dependent problems with small failure probability, Reliability Engineering & System Safety 219 (2022) 108230.

[11] Y. M. Liu, S. Mahadevan, Efficient methods for time-dependent fatigue reliability analysis, Aiaa Journal 47 (3) (2009) 494–504.

[12] Y. Dong, A. Teixeira, C. Guedes Soares, Time-variant fatigue reliability assessment of welded joints based on the phi2 and response surface methods, Reliability Engineering & System Safety 177 (2018) 120–130.

[13] Y. Dong, A. Teixeira, C. Guedes Soares, Application of adaptive surrogate models in time-variant fatigue reliability assessment of welded joints with surface cracks, Reliability Engineering & System Safety 195 (2020) 106730.

[14] Rice, O. S., Mathematical analysis of random noise, Bell System Technical Journal 24 (1945) 46–156.

[15] C. Andrieu-Renaud, B. Sudret, M. Lemaire, The phi2 method: a way to compute time-variant reliability, Reliability Engineering and System Safety 84 (2004) 75–86.

[16] L. D. Lutes, S. Sarkani, Reliability analysis of systems subject to first-passage failure, NASA technical report No.504 NASA/CR-2009-215782 (2009).

[17] K. Breitung, Asymptotic crossing rates for stationary gaussian vector processes, Stochastic Processes and their Applications 29 (1988) 195–207.

[18] Øistein Hagen, Threshold up-crossing by second order methods, Probabilistic Engineering Mechanics 7 (1992) 235 – 241.

[19] S. Engelund, R. Rackwitz, C. Lange, Approximations of first-passage times for differentiable processes based on higher-order threshold crossings, Probabilistic Engineering Mechanics 10 (1995) 53–60.

[20] P. Madsen, S. Krenk, An integral equation method for the first-passage problem in random vibration, Journal of Applied Mechanic 51 (1984) 674–679.

[21] Øistein Hagen, L. Tvedt, Vector process out-crossing as parallel system sensitivity measure, Journal of Engineering Mechanics 117 (1991) 2201–2220.

[22] B. Sudret, Analytical derivation of the outcrossing rate in time-variant reliability problems, Structure and Infrastructure Engineering 4 (2008) 353–362.

[23] Z. Hu, X. Du, Time-dependent reliability analysis with joint upcrossing rates, Structural & Multidiplinary Optimization 48 (2013) 893–907.

[24] O. D. Ditlevsen, H. O. Madsen, Structural reliability methods (1996).

[25] X.-Y. Zhang, Z.-H. Lu, S.-Y. Wu, Y.-G. Zhao, An efficient method for time-variant reliability including finite element analysis, Reliability Engineering & System Safety 210 (2021) 107534.

[26] X.-W. Li, Y.-G. Zhao, X.-Y. Zhang, Z.-H. Lu, Explicit model of outcrossing rate for time-variant reliability, ASCE-ASME Journal of Risk and Uncertainty in Engineering Systems, Part A: Civil Engineering 8 (1) (2022) 04021087.

[27] Z. Wang, W. Chen, Time-variant reliability assessment through equivalent stochastic process transformation, Reliability Engineering & System Safety 152 (2016) 166–175.

[28] Z. Wang, P. Wang, A nested extreme response surface approach for time-dependent reliability-based design optimization, Journal of Mechanical Design 134 (2012) 121007.

[29] Z. Hu, X. Du, Mixed Efficient Global Optimization for Time-Dependent Reliability Analysis, Journal of Mechanical Design 137 (2015) 051401.

[30] Z. Wang, W. Chen, Confidence-based adaptive extreme response surface for time-variant reliability analysis under random excitation, Structural Safety 64 (2017) 76–86.

[31] L. Hawchar, C.-P. El Soueidy, F. Schoefs, Principal component analysis and polynomial chaos expansion for time-variant reliability problems, Reliability Engineering & System Safety 167 (2017) 406–416.

[32] H.-M. Qian, Y.-F. Li, H.-Z. Huang, Time-variant system reliability analysis method for a small failure probability problem, Reliability Engineering & System Safety 205 (2021) 107261.

[33] H.-M. Qian, T. Huang, H.-Z. Huang, A single-loop strategy for time-variant system reliability analysis under multiple failure modes, Mechanical Systems and Signal Processing 148 (2021) 107159.

[34] Z. Hu, S. Mahadevan, Time-dependent reliability analysis using a vine-arma load model, Asce-Asme Journal of Risk and Uncertainty in Engineering Systems Part B-Mechanical Engineering 3 (1) (2017).

[35] Z. Hu, X. Du, A Sampling Approach to Extreme Value Distribution for Time-Dependent Reliability Analysis, Journal of Mechanical Design 135 (2013) 071003.

[36] M. Ping, X. Han, C. Jiang, X. Xiao, A time-variant extreme-value event evolution method for time-variant reliability analysis, Mechanical Systems and Signal Processing 130 (2019) 333–48.

[37] G. Jia, P. Gardoni, State-dependent stochastic models: A general stochastic framework for modeling deteriorating engineering systems considering multiple deterioration processes and their interactions, Structural Safety 72 (2018) 99–110.

[38] M. Sanchez-Silva, G.-A. Klutke, D. V. Rosowsky, Life-cycle performance of structures subject to multiple deterioration mechanisms, Structural Safety 33 (3) (2011) 206–217.

[39] R. Kumar, D. B. Cline, P. Gardoni, A stochastic framework to model deterioration in engineering systems, Structural Safety 53 (2015) 36–43.

[40] C. Wang, H. Zhang, Q. Li, Reliability assessment of aging structures subjected to gradual and shock deteriorations, Reliability Engineering & System Safety 161 (2017) 78–86.

[41] C. Wang, An explicit compound poisson process-based shock deterioration model for reliability assessment of aging structures, Journal of Traffic and Transportation Engineering (English Edition) (2021).

[42] D. Straub, R. Schneider, E. Bismut, H.-J. Kim, Reliability analysis of deteriorating structural systems, Structural Safety 82 (2020) 101877.

[43] Q. Zhou, Z. Li, W. Fan, A. H.-S. Ang, R. Liu, System reliability assessment of deteriorating structures subjected to time-invariant loads based on improved moment method, Structural Safety 68 (2017) 54–64.

[44] Y. Yang, J. Peng, C. Cai, Y. Zhou, L. Wang, J. Zhang, Time-dependent reliability assessment of aging structures considering stochastic resistance degradation process, Reliability Engineering & System Safety 217 (2022) 108105.

[45] K. Cheng, Z. Lu, Time-variant reliability analysis based on high dimensional model representation, Reliability Engineering and System Safety 188 (2019) 310–319.

[46] C. Li, A. Der Kiureghian, Optimal discretization of random fields, Journal of Engineering Mechanics Asce 119 (1993) 1136–1154.

[47] B. Sudret, A. Der Kiureghian, Stochastic finite element methods and reliability a state-of-the-art report 08 (2000).

[48] J. Zhang, B. Ellingwood, Orthogonal series expansions of random fields in reliability analysis, Journal of Engineering Mechanics 120 (1994) 2660–2677.

[49] L. MM, Probability theory i, Graduate Texts in Mathematics II (1977) 378–382.

[50] K. Phoon, H. Huang, S. Quek, Comparison between karhunen–loeve and wavelet expansions for simulation of gaussian processes, Computers & Structures 82 (2004) 985–991.

[51] K. Phoon, S. Huang, S. Quek, Simulation of second-order processes using karhunen–loeve expansion, Computers & Structures 80 (2002) 10499–1060.

[52] L. Li, K. Phoon, S. Quek, Comparison between karhunen–loève expansion and translation-based simulation of non-gaussian processes, Computers & Structures 85 (2007) 264–276.

[53] J.-B. Chen, J. Li, The extreme value distribution and dynamic reliability analysis of nonlinear structures with uncertain parameters, Structural Safety 29 (2007) 77–93.

[54] J. B. Chen, M. Z. Lyu, A new approach for time-variant probability density function of the maximal value of stochastic dynamical systems, Journal of Computational Physics 415 (2020) 109525.

[55] G. E. P. Box, D. R. Cox, An analysis of transformations, Journal of the Royal Statistical Society: Series B (Methodological) 26 (1964) 211–243.

[56] C. H. Cai, Z. H. Lu, Y. G. Zhao, Moment method with box–cox transformation for structural reliability, Journal of Engineering Mechanics 146 (2020) 04020086.

[57] P. L. Novi Inverardi, A. Tagliani, Maximum entropy density estimation from fractional moments, COMMUNICATIONS IN STATISTICS Theory and Methods Vol. 32 No. 2 (2003) 327–345.

[58] Hausdorff moment problem and fractional moments: A simplified procedure, Applied Mathematics and Computation 218 (2011) 4423–4432.

[59] J. Xu, C. Dang, F. Kong, Efficient reliability analysis of structures with the rotational quasi-symmetric point- and the maximum entropy methods, Mechanical Systems and Signal Processing 95 (2017) 58–76.

[60] J. Xu, F. Kong, Adaptive scaled unscented transformation for highly efficient structural reliability analysis by maximum entropy method, Structural Safety 76 (2019) 123–134.

[61] G. Li, H. Wanxin, Y. Zeng, An improved maximum entropy method via fractional moments with laplace transform for reliability analysis, Structural and Multidisciplinary Optimization 59 (2019) 1301–1320.

[62] J. Xu, C. Dang, A novel fractional moments-based maximum entropy method for high-dimensional reliability analysis, Applied Mathematical Modelling 75 (2019) 749–768.

[63] S. He, J. Xu, Y. Zhang, Reliability computation via a transformed mixed-degree cubature rule and maximum entropy,

Applied Mathematical Modelling 104 (2022) 122–139.
[64] C. Dang, J. Xu, Unified reliability assessment for problems with low- to high-dimensional random inputs using the laplace transform and a mixture distribution, Reliability Engineering & System Safety 204 (2020) 107124.
[65] H. Gzyl, P. Novi Inverardi, A. Tagliani, Entropy and density approximation from laplace transforms, Applied Mathematics & Computation 265 (2015) 225–236.
[66] J. Xu, S. Zhu, An efficient approach for high-dimensional structural reliability analysis, Mechanical Systems and Signal Processing 122 (2019) 152–170.
[67] J. Chen, J. Yang, J. Li, A gf-discrepancy for point selection in stochastic seismic response analysis of structures with uncertain parameters, Structural Safety 59 (2016) 20–31.
[68] J. Xu, F. Kong, A new unequal-weighted sampling method for efficient reliability analysis, Reliability Engineering & System Safety 172 (2018) 94–102.
[69] S. Marelli, B. Sudret, Uqlab: A framework for uncertainty quantification in matlab, in: Vulnerability, Uncertainty, and Risk: Quantification, Mitigation, and Management (2014) 2554–2563.
[70] B. Sudret, G. Defaux, C. Andrieu, Comparison of methods for computing the probability of failure in time-variant reliability using the outcrossing approach, Computational Stochastic Mechanics (2003) 609–618.
[71] S.-K. Au, J. L. Beck, Estimation of small failure probabilities in high dimensions by subset simulation, Probabilistic Engineering Mechanics 16 (4) (2001) 263–277.
[72] H. S. Li, T. Wang, J. Y. Yuan, H. Zhang, A sampling-based method for high-dimensional time-variant reliability analysis, Mechanical Systems & Signal Processing 126 (2019) 505–520.
[73] X. Chen, Z. Lin, Structural nonlinear analysis program opensees theory and tutorial, Beijing: China Architecture & Building Press (2014) 212–219.
[74] Titi, Andrea, Biondini, Fabio, On the accuracy of diffusion models for life-cycle assessment of concrete structures, Structure & Infrastructure Engineering 9 (2016) 1202–1215.
[75] J. Li, J. Chen, Stochastic dynamics of structures, John Wiley & Sons (2009).